DISSERTATIONES
GEOGRAPHICAE
UNIVERSITATIS
TARTUENSIS
92

SANDEEP THAYAMKOTTU

Ecosystem scale modelling of carbon and nitrogen cycles in peatlands

DISSERTATIONES GEOGRAPHICAE UNIVERSITATIS TARTUENSIS
92

DISSERTATIONES GEOGRAPHICAE UNIVERSITATIS TARTUENSIS
92

SANDEEP THAYAMKOTTU

Ecosystem scale modelling of carbon and nitrogen cycles in peatlands

UNIVERSITY OF TARTU
Press
1632

Department of Geography, Institute of Ecology and Earth Sciences, Faculty of Science and Technology, University of Tartu, Estonia

The dissertation was accepted for the commencement of the degree of *Doctor philosophiae* in physical geography at the University of Tartu on 21 May 2025 by the Scientific Council of the Institute of Ecology and Earth Sciences University of Tartu.

Supervisors: Assoc. Prof. Jaan Pärn
Institute of Ecology and Earth Sciences, Department of Geography, University of Tartu, Estonia

Prof. Ülo Mander
Institute of Ecology and Earth Sciences, Department of Geography, University of Tartu, Estonia

Dr. Thomas Luke Smallman
Research Fellow
School of GeoSciences & National Centre for Earth Observation, The University of Edinburgh, Scotland, UK

Opponent: Dr. Avni Malhotra
Earth Scientist
Biological Sciences Division
Pacific Northwest National Laboratory
Richland, Washington, USA

Commencement: Senate Hall, University Main Building, Ülikooli 18, Tartu, on June 26, 2025, at 14:15.

Publication of this dissertation is granted by the Institute of Ecology and Earth Sciences, University of Tartu.

ISSN 1406-1295 (print)
ISBN 978-9916-27-899-4 (print)
ISSN 2806-2302 (pdf)
ISBN 978-9916-27-900-7 (pdf)

University of Tartu Press
www.tyk.ee

CONTENTS

ORIGINAL PUBLICATIONS

This thesis is based on the following publications which are referred to in the text by Roman numerals. Published papers are reproduced in print with the permission of the publisher.

I. Pärn, J., **Thayamkottu, S.,** Öpik, M., Bahram, M., Tedersoo, L., Espenberg, M., Davison, J. A., Kasak, K., Maddison, M., Niinemets, Ü., Ostonen, I., Soosaar, K., Zobel, M., & Mander, Ü. (2025) Soil moisture and microbiome explain greenhouse gas exchange in global peatlands, *Scientific Reports, 15*(1), 10153. https://doi.org/10.1038/s41598-025-92891-z

II. Pärn, J., Espenberg, M., Soosaar, K., Kasak, K., **Thayamkottu, S**., Schindler, T., Ranniku, R., Sohar, K., Malaverri, L. F., Melling, L., & Mander, Ü. Importance of N_2O in greenhouse gas budgets of tropical peatlands, (Submitted).

III. **Thayamkottu, S**., Smallman, T. L., Pärn, J., Mander, Ü., Euskirchen, E. S., & Kane, E. S. (2024) Greening of a boreal rich fen driven by CO_2 fertilisation. *Agricultural and Forest Meteorology*, *359*, 110261. https://doi.org/10.1016/j.agrformet.2024.110261

IV. **Thayamkottu, S.,** Masta, M., Skeeter, J., Pärn, J., Knox, S. H., Smallman, T. L., & Mander, Ü. (2025) Dual controls of vapour pressure deficit and soil moisture on photosynthesis in a restored temperate bog, *Science of the Total Environment*, *963,* 178366. https://doi.org/10.1016/j.scitotenv.2024.178366

Author's contribution to the articles denotes: '*' a minor contribution, '**' a moderate contribution, '***' a major contribution.

Categories	Author's contribution			
	I	II	III	IV
Original idea	*	*	***	***
Study design	*	*	***	***
Data processing and analysis	***	***	***	***
Interpretation of the results	**	**	***	***
Writing the manuscript	**	**	***	***

Department of Geography, Institute of Ecology and Earth Sciences, Faculty of Science and Technology, University of Tartu, Estonia.

ABBREVIATIONS AND ACRONYMS

Abbreviation	Definition
C	Carbon
CARDAMOM	Carbon data model fusion framework
CCM	Convergent cross mapping
CH_4	Methane
CI	Confidence interval
CO_2	Carbon dioxide
DALEC	Data Assimilation Linked Ecosystem Carbon model
EC	Eddy covariance
EDC	Ecological and dynamical constraints
EDM	Empirical dynamic modelling
EF	Evaporative fraction
EO	Earth observation
ET	Evapotranspiration
FRC	Fine root carbon
G_{sw}	Bulk surface conductance
GAM	Generalised additive model
GHG	Greenhouse gases
GPP	Gross primary productivity
GWC	Gravimetric water content
GWP	Global warming potential
IAV	Inter-annual variation
LAI	Leaf area index
LULCC	Land use land cover change
MC	Moisture coefficient
MDF	Model–data fusion framework
N	Nitrogen
N_2	Dinitrogen
N_2O	Nitrous oxide
NEE	Net ecosystem exchange
NH_4^+	Ammonium
NO_3^-	Nitrate
NPP	Net primary productivity
PET	Potential evapotranspiration
R_a	Autotrophic respiration
R_h	Heterotrophic respiration
RDA	Redundancy analysis
SE	Standard error
SOC	Soil organic carbon
SPEI	Standardised precipitation evapotranspiration index
SWC	Soil water content
VPD	Vapour pressure deficit
WTD	Water table depth

ABSTRACT

Peatlands, despite covering ~3% of the global land surface area, harbour a third of the global soil organic carbon (C) pool and ~15% of the global soil nitrogen. Climate change and land use land cover changes have put these natural C sinks under pressure. Projected increase in global warming-driven climate extremes and subsequent climate–carbon feedbacks may turn peatlands into sources of carbon dioxide (CO_2) and nitrous oxide (N_2O): the two potent greenhouse gases. But we still lack a consensus on the land–atmosphere exchange of CO_2 (gross primary productivity (GPP) and net ecosystem exchange (NEE)) and N_2O fluxes under changing climate and extreme events. Removing the uncertainties of greenhouse gas (GHG) exchange, especially C in the soil–plant–atmosphere continuum requires a mechanistic and holistic of the C cycle processes and their drivers in peatlands. In this context, this thesis explores filling the knowledge gaps in drivers of (primarily) CO_2 and N_2O exchange in the soil–plant–atmosphere continuum. To that extent, the thesis asks the following research questions.

1. What is the state of GHG exchange in the world's open peatlands (Article I) and tropical peatlands? (Article II)
2. What drives the GHG exchange? (Articles I and II)
3. What drives the ecosystem scale inter-annual variability of CO_2 fluxes? (Article III)
4. What are C allocation patterns during the study years? (Article III)
5. How does atmospheric drought impact evapotranspiration and GPP in a restored peatland? (Article IV)
6. Is there a threshold at which soil water content (SWC) starts to regulate GPP? (Article IV)

The analysis conducted in Articles I and II found that CO_2 fluxes dominated GHG exchange across 48 open peatlands worldwide. SWC was the dominant abiotic factor that drove the GHG dynamics and net ecosystem exchange of CO_2. Evidence of a Gaussian relationship between SWC and NEE and GHG was found in the first two articles. The peaks were emissions at 0.4 m^3 m^{-3} to 0.7 m^3 m^{-3} SWC. Dry and wet regions were sinks of CO_2. Prokaryotic abundances, especially bacterial abundances, were the second most important factor for GHG and CO_2 dynamics in the soils. Article III did not find any relationship between GPP, and NEE with SWC. Furthermore, using a terrestrial ecosystem model of CO_2 calibrated with a Bayesian approach, Article III found a CO_2 fertilisation effect on a sub-Arctic rich fen peatland. During the seven-year study period, foliage allocation was favoured over other plant tissues on average. In Article IV, a dynamic of energy and water limitation of GPP in a drought-affected temperate bog peatland was found. Specifically, SWC started limiting GPP as it dropped below 82.5% of the field capacity; –8cm water table depth. These findings lead to the hypothesis of the existence of complex regional and/or biome specific soil moisture relationship with GPP and NEE. Warming (Article III) and associated extreme events (Article IV) can amplify or diminish the hydro-climatic impacts.

1. INTRODUCTION

Peatlands have been an important component of the land carbon (C) sink since the Holocene and contributed to negative net radiative forcing (RF) (–0.2 W m^{-2} to –0.5 W m^{-2}). Globally, peatlands have accumulated ~850 Pg C during the Holocene, despite covering ~3% of the global land surface area (Chaudhary et al., 2020; Yu, 2011; Yu et al., 2010). Consequently, peat still stores ~560 Pg C which is more than terrestrial vegetation (Spawn et al., 2020; Turetsky et al., 2015). This is fuelled by the imbalance between the production and decay rates of C from the reduced soil microbial activity in the hypoxic peat soils. Organic soils also store ~15% of the global soil nitrogen (N) pool (Batjes, 2014). On the other hand, peatlands are natural sources of methane (CH_4) accounting for ~20% of the global CH_4 emissions (Bloom et al., 2010). The interactions of these potent greenhouse gases (GHG) between and with the vegetation, meteorological drivers and microbes are unequivocally imperative in understanding peatland ecosystems and their future.

1.1. C and N cycles in peatlands

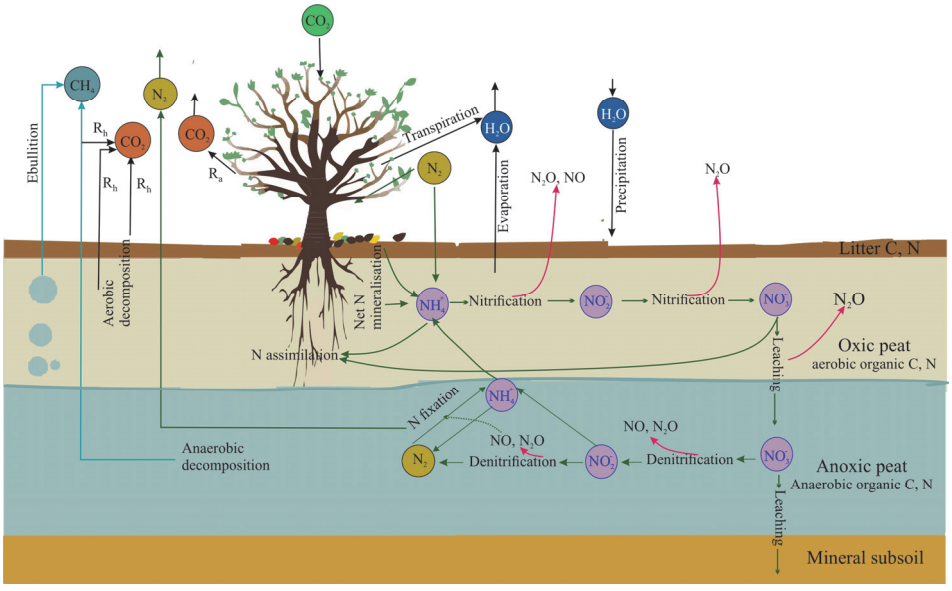

Figure 1: Biogeochemical cycles and related key processes

Terrestrial vegetation fixes C from the atmosphere (gross primary productivity (GPP)) by photosynthesis. Plants respire a part of the GPP back to the atmosphere due to spending energy on the growth and maintenance of plant tissues (autotrophic respiration (R_a)). The remainder (net primary productivity (NPP)) allocated to different live biomass pools. These are foliage, aboveground, below-

ground, and labile C pool. As the plant tissues die (leaf fall, branches, stem and root residue), a part of the C is released in the form of heterotrophic respiration (R_h) from the litter by aerobic decomposition. The remainder is added to the soil organic carbon (SOC) pool. Peatlands differ from other biomes due to their saturated soils (Kettridge & Waddington, 2014; Weiss et al., 1998). It leads to a reduction in aerobic decomposition and consequently a decline in R_h (Figure 1). This creates a discrepancy between GPP and decomposition rates which provides ambient microclimate for peat accumulation (Kleinen et al., 2012; Nichols & Peteet, 2019; Turetsky et al., 2015; Yu, 2011).

Oxic and anoxic peat layers mediate multiple microbe-driven assimilative and dissimilative N cycle processes (Figure 1). Atmospheric dinitrogen (N_2) is not readily available for plant intake. There are two processes where atmospheric N_2 can be converted into plant-available N. These are N fixation and mineralisation (Figure 1). First, atmospheric N_2 is fixed by free-living bacteria to ammonium (NH_4^+). Plants assimilate a part of the NH_4^+ from the oxic peat soils. The remainder is converted into nitrate (NO_3^-) by a process called nitrification. First, NH_4^+ is converted into nitrite (NO_2^-). In the second step, NO_2^- is oxidised into plant available N form: NO_3^-. Furthermore, incomplete nitrification can emit nitrous oxide (N_2O) and nitrogen monoxide (NO). The remaining NO_3^- from the plant assimilation leach to the anoxic layer and then to the mineral subsoil. In the process, a part of it is lost back to the atmosphere as N_2O. In the anoxic peat layers NO_3^- is converted into N_2 by a two-step process called denitrification. Denitrification is exclusively carried out in anaerobic conditions. In the end, N_2O is removed from the ecosystem as N_2. Thus, N is easily available for plant and microbial uptake.

Anaerobic decomposition in peat soils is a major biogenic source of CH_4 and is considered the primary driver of inter-annual variations in atmospheric CH_4 growth rate (Nisbet et al., 2014; Qiu et al., 2020). The opposite directions of carbon dioxide (CO_2) and CH_4 exchanges create uncertainty around the net C balance of peatlands. However, the climatic effects of CH_4 can be outweighed by net CO_2 uptake and storage over longer time scales (Frolking et al., 2011). However, since industrialisation, anthropogenic and climate change impacts have widely altered global peatlands' CO_2 sink strength (Leifeld & Menichetti, 2018).

1.2. Fate of peatlands under climate change

1.2.1. Anthropogenic and climate warming impacts on peat soils (Articles I & II)

Land use and land cover change (LULCC), and global warming are the prominent sources of CO_2 emissions. However, constraining C emissions remains a challenge due to uncertainties around GHG emissions in peatlands (Günther et al., 2020; Petrescu et al., 2015). The knowledge gaps in ecosystem responses to climate warming and peat drainage drive this. A lack of holistic process-based

appraisal of peatland C and N cycles further contributes to the uncertainties of the global C cycle. Peatlands have been drained for agriculture, forestry, and peat extraction for decades. This can result in increased emissions from the current peatland area (~3% of the global land surface area; Loisel et al., 2014; Yu, 2011)). These changes are primarily attributed to the northern hemisphere. Drainage of this magnitude impedes peatland ecosystem services. Peat oxidation is responsible ~5% direct GHG emissions (Günther et al., 2020; Leifeld & Menichetti, 2018). Unrestrained peatland emissions may constitute 12% to 41% of the total GHG budget until 2100 for keeping global warming below +1.5 °C to +2.0 °C (Leifeld et al., 2019). On the other hand, the indirect impacts of drainage and oxidation on C and N cycle processes and broader ecosystem responses are still not fully understood. If the drainage continues uninterrupted, the instantaneous RF could increase (~0.15 W m^{-2}) by 2100 (Günther et al., 2020). Yet, the balance between GHG fluxes and their drivers in open peatlands (No tree cover and Vegetation height < 5m) remains poorly understood.

The modulating effects of soil water content (SWC), temperature and nutrients on soil GHG fluxes are still debated. While several studies suggest a positive response of GHG to SWC drawback (Evans et al., 2021; Huang et al., 2021; Jauhiainen et al., 2005), contradicting evidence was also reported (Pärn et al., 2018; Quan et al., 2019). Similar contradicting findings were reported for temperature (Gougoulias et al., 2014; Muller et al., 2015; Murdiyarso et al., 2010; Pärn et al., 2018; Treat et al., 2019; Yavitt et al., 1997) and availability of N (Bardgett et al., 2003; De Deyn et al., 2008; Kaye & Hart, 1997). Climate warming and LULCC further amplify these effects and can have long-term implications (Leifeld et al., 2019; Limpens et al., 2008; Murdiyarso et al., 2010). As the primary producers, plants and their responses to climate warming, drainage, and extreme events are unequivocally important in understanding such implications.

1.2.2. Plants' role in peatland C balance under climate change (Articles III & IV)

GPP is of paramount importance in C accumulation and appraisal of terrestrial C dynamics (Grossiord et al., 2020; Kwon et al., 2022; López et al., 2021; Novick et al., 2016, 2024; Peichl et al., 2018; Perez-Quezada et al., 2024). Plant water-C coupling and its drivers play a critical role in regulating GPP. There are two crucial points of water-C coupling: in the roots and the stomata (Gentine et al., 2019). The stomata are where atmospheric CO_2 enters the leaf for carboxylation and, in the process, transpires water back into the atmosphere. These processes are heavily dependent on the climate, species, ecosystem state and vice versa (Bassiouni et al., 2020; Grossiord et al., 2020; López et al., 2021; Zarakas et al., 2020). A consensus has not yet been reached on how these processes are impacted by peatland drainage, LULCC and global warming. Warming could prolong the growing season, trigger rapid thaw, shorten the winter season and cause flooding

during the growing season. The sources and timing of the flood events can have a significant impact on GPP and inter-annual variation (IAV) of C (Euskirchen et al., 2020). For example, water table drawdown could trigger enhanced decomposition or GPP, shifts in phenology and community structure (Antala et al., 2022; Davidson et al., 2021; Guay et al., 2014; Peichl et al., 2018; Wilkinson et al., 2023). Satellite and model-based photosynthetic capacity assessments have shown an increase in GPP and potentially associated increases in biomass, canopy cover and leaf area (Berner et al., 2020; Guay et al., 2014; Ju & Masek, 2016; Myers-Smith et al., 2020). However, a warming-induced browning was also reported in parts of the high-latitude ecosystems (Myers-Smith et al., 2020; Phoenix & Bjerke, 2016).

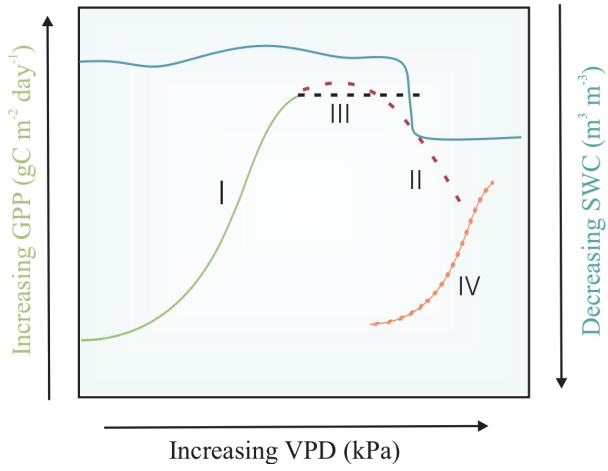

Figure 2: A conceptual diagram portraying ecosystem GPP responses to changes in VPD and SWC. Here four probable GPP responses (marked in Roman numerals I through IV) to changes in VPD and SWC are shown. 1 (Green line): GPP increases with an increase in VPD under normal VPD and SWC. II (Red dotted line): Partial or complete stomatal closure to preserve water leads to a sudden de- cline in GPP. III (Black dotted line): Under increased VPD (increased atmospheric water demand), ecosystems tend to increase intrinsic water use efficiency to maximise C assimilation. This results in a constant GPP value. IV (Orange dotted line): With frequent droughts, the ecosystem chooses an alternate steady state where the GPP-VPD relationship mimics I. But photosynthetic efficiency (unit C fixed per unit leaf area) is reduced compared to I. (Source: Article III)

Peatland C – water exchanges are further complicated by the presence of sphagnum moss, which lacks stomata, and instead has passive capillary action for water transport and water retention characteristics (Kettridge & Waddington, 2014; Kim & Verma, 1996; Nichols & Brown, 1980; Price, 1997; Thompson & Waddington, 2008). But climate warming and increases in the severity of extreme events threaten to alter plant water–C coupling and GPP in peatlands (Freeman et al., 2022; Frolking et al., 2011; Turetsky et al., 2015). Climate change is causing the severity and frequency of droughts to increase in the northern hemisphere, where most peatlands are located (IPCC, 2023). Droughts can also

cause or combine with fire, resulting in a cascade of damage responses (Tschumi et al., 2022). For instance, severe atmospheric droughts trigger SWC decline due to increased atmospheric water demand (i.e., vapour pressure deficit (VPD)), exposing peat soils to oxygen and releasing CO_2 (Fenner & Freeman, 2011). An increase in VPD has also been shown to reduce GPP under severe droughts because vascular plants close their stomata to prevent further water loss (Figure 2; Line II. A change from linear positive relationship (Line I)) (Breshears et al., 2013). Accordingly, the ecosystem fails to meet the atmospheric water demand.

Plants can also increase their intrinsic water use efficiency (i.e. the ratio of C gained to water lost through stomata) by stomatal regulation to maximise C assimilation (Figure 2; Line III) under increased VPD (Zhang et al., 2016). However, the role of SWC in GPP is still debated. While some studies suggested the presence of SWC limitation (Voigt et al., 2024; Wang et al., 2022), Zhang et al., (2016) showed the absence of SWC limitation. In peatlands, SWC-GPP dynamics is more involved because mosses (if present) cannot prevent water loss (Admiral & Lafleur, 2007; Williams & Flanagan, 1996), resulting in desiccated and compressed mosses under droughts (Dorrepaal et al., 2004; Nichols & Brown, 1980; Thompson & Waddington, 2008). This, combined with soil texture properties, prevents soil evaporation because of a decline in capillary rise, causing the hysteresis between SWC and evapotranspiration (ET), culminating in lagged responses of GPP and stomatal or canopy regulations to drought. As the water table depth (WTD) drops, the peat and ecosystem properties change with prolonged droughts. These changes can push the ecosystem to an alternate steady state (Figure 2; Line IV), such as shrub dominance, which can also support C accumulation in peatlands (Wang et al., 2015).

Despite a multitude of literature covering the C and N cycle dynamics in the soil-plant-atmosphere continuum, their drivers and domino effects of climate-carbon feedback are still poorly understood. To improve predictions of both C and N cycle dynamics in peatlands, major weaknesses in soil and plant-related processes must be solved. Improving the process-based models based on empirical knowledge retrieved from site and ecosystem scale investigations is imperative. This would, in turn, reduce the uncertainties in the C and N exchange in peatlands.

The aim of this thesis is to fill some of the knowledge gaps found in the literature by investigating the following research questions and respective scientific hypotheses.

1. What is the state of GHG exchange in the world's open peatlands (Article I) and tropical peatlands? (Article II)
   - CO_2 fluxes dominated the GHG exchange and N_2O was the dominant GHG
2. What drives the aforementioned GHG exchange? (Articles I and II)
   - Abiotic factors (SWC and temperature) are the most important drivers of GHG exchange.

3. What drives the ecosystem scale IAV of CO_2 fluxes? (Article III)
   - Production has increased due to CO_2 fertilisation.
4. What are the internal C allocation patterns during the study years? (Article III)
   - Fractional allocation of photosynthate will be greater to foliage than fine root.
5. How does atmospheric drought impact ET and GPP in a restored peatland? (Article IV)
   - G_{sw} started declining with increasing drought severity due to physiological regulations leading to plant water stress (Figure 2; Line II).
6. Is there a threshold at which SWC drawback starts to regulate GPP? (Article IV)
   - The variation in SWC beyond a point causes GPP to be regulated by SWC more than VPD.

2. MATERIALS AND METHODS

This thesis employs three distinct approaches to comprehensively analyse the hydro-climatic impact on terrestrial GHG exchange, especially CO_2. I started by investigating the three GHG fluxes and their biotic and abiotic drivers, such as microbes and climatic factors across the selected global and tropical peatlands (Articles I and II). The next two articles (Articles III and IV) set to improve on the obtained empirical knowledge of terrestrial C cycle from Articles I and II. I have also addressed the process-based limitations of C cycling, and its coupling with water cycle in Articles III and IV. Article III focused on CO_2 dynamics and its allocation patterns by employing an intermediate complexity process-based model called Data Assimilation Linked Ecosystem Carbon model (DALEC) version 2 (Bloom et al., 2016; Williams et al., 2005) calibrated by a Bayesian calibration approach called the carbon data model framework (CARDAMOM) (Bloom et al., 2016; Bloom & Williams, 2015). Finally, in the fourth paper, coupling and interaction of C and water cycles were investigated using a data-driven model embedded in chaos theory (Deyle et al., 2016; Deyle & Sugihara, 2011; Sugihara et al., 1997, 2012). The study sites, approaches, data, and sampling schemes are outlined below.

2.1. Soil moisture governs C and N fluxes in global peatlands (Articles I & II)

2.1.1. Statistical analysis

First, I investigated how GHG and specifically NEE respond to changes across the SWC gradient (dry to wet) using the in-situ measurements from 48 open peatlands sites (i.e., with vegetation height <0.5 m, Figure 3). The field campaign was conducted by my supervisors and colleagues between 2011 and 2018. The survey included sampling of CO_2, CH_4, and N_2O fluxes and potentially controlling environmental variables during the dry season (i.e. the annual water table minimum, including temperate and boreal summers). The sites are spread throughout the rainy tropical (A), temperate (C), and boreal (D) climate zones of the Köppen classification. The natural and artificially drained sites were identified based on the proximity of drainage ditches, WTD, and characteristic vegetation. The hydrology and trophic status of the natural sites ranged from groundwater-fed swamps and fens to rain-fed peat bogs. To capture the whole variety of GHG fluxes at a site, transects of 2 to 3 plots were set up, each containing 3 to 4 opaque chambers arranged along 25 to 100 m terrain. The gas from the chambers was sampled during 3- to 6-day campaigns. The ecosystem respiration (noted as ER in Articles I & II and Reco in Articles III & IV; in mg CO_2 m^{-2} h^{-1}), CH_4 and N_2O fluxes (in mg m^{-2} h^{-1}) were estimated from the samples using a gas chromatograph (Pärn et al., 2018).

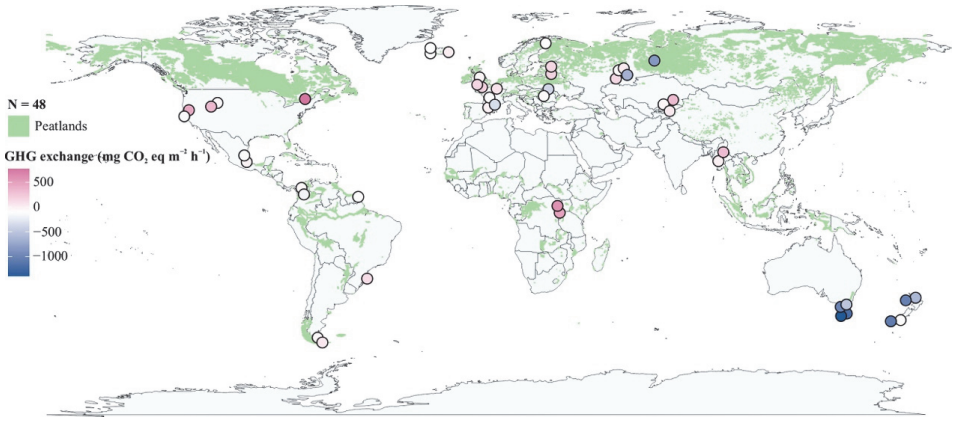

Figure 3: Global open peatland study sites and their GHG balance. (Source: Article I)

First, I calculated net ecosystem exchange (NEE) following eq (2.1):

$$NEE = ER - GPP \tag{2.1}$$

I used the MOD17A2H V006 data (Running et. al., 2015) developed from the moderate resolution imaging spectroradiometer sensor onboard the Terra and Aqua remote sensing satellites (expressed in mg CO_2 m^{-2} h^{-1}). Next, I calculated GHG exchange for each chamber following eq 2.2.

$$GHG\ exchange = CH_4 \times GWP_{CH_4} + N_2O \times GWP_{N_2O} + NEE \tag{2.2}$$

Where GHG exchange is the greenhouse gas exchange in CO_2 equivalents (CO_2eq). CO_2eq of N_2O and CH_4 was calculated by multiplying the respective gases with their global warming potential (GWP). CH_4 is the field-observed methane flux. GWP_{CH_4} is 28 CO_2eq (the 100-year global warming potential of CH_4 without climate-carbon feedback (IPCC, 2023). N_2O is the field-observed N_2O flux, GWP_{N_2O} is 265 CO_2eq; the 100-year global warming potential of N_2O without climate-carbon feedback (IPCC, 2023). NEE is the net ecosystem exchange of CO_2 (Eq 2.1).

This approach was followed because the 48 sites did not have any tree cover and were homogenous, and thus significantly reduces the probability of over estimation (Lees et al., 2019) and underestimation (Wang et al., 2017). Additionally, Watts et al., (2021) compare multiple scale varying datasets against chamber and eddy covariance (EC) based soil respiration data in the Arctic-boreal zone peatlands. They reported the moderate resolution imaging spectroradiometer GPP as the strongest predictor of soil respiration (consist of both chamber and EC dataset) at site scale during the summer amongst other large-scale variables including enhanced vegetation index estimates based on LANDSAT 30 m dataset, and sand content estimates from the SoilGrids dataset (250 m; Poggio et al., 2021). Similar comparisons of EC tower and chamber-based respiration

fluxes with MODIS GPP datasets were made by Niu et al., (2017) as well. Consequently, GPP units were converted from g C m^{-2} 8 $days^{-1}$ to mg C m^{-2} h^{-1} for comparability with the chamber measured ER.

Organic matter content of dry matter was determined by loss on ignition (Bahram et al., 2022; Pärn et al., 2018). SWC was determined from gravimetric water content (GWC), dry matter content and empirically established bulk densities of mineral and organic matter fractions using the following procedure (Pärn et al., 2018). GWC was determined as the difference between fresh and oven-dry weight divided by oven-dry weight. Bulk density was determined using eq 2.3 below.

$$BD = (D_{bm} \times D_{bo})/(SOM \times D_{bm} + (1 - SOM) \times D_{bo}) \quad (2.3)$$

BD is bulk density in Mg m^{-3}. D_{bm} is the empirically determined bulk density of the mineral fraction (2.65 Mg m^{-3}) (Périé & Ouimet, 2008). D_{bo} is the empirically determined bulk density of the organic fraction (0.035 to 0.23 Mg m^{-3} according to the von Post humification scale, which is a field test to rank organic soils by degree of decomposition (see von Post & Granlund (1926) and FAO (2011) for more details on the classification criteria) (Silc & Stanek, 1977). SOM is the organic content of oven-dry soil, Mg Mg^{-1}. Finally, SWC was determined using the equation below.

$$SWC = GWC \times BD \quad (2.4)$$

Next, I fitted linear and non-parametric generalised additive models (GAM) after assessing the normality of the data. Where necessary, the data was log-transformed. For the GHG flux rates, environmental predictor variables: soil and water temperature, distance from the equator, Köppen climate zone (A, C or D), water table, SWC, soil chemistry (pH, total C%, total N%, C:N ratio, organic matter, ammonium, nitrate, calcium, magnesium, phosphorus and potassium), water oxygen content and agricultural land use intensity, were considered.

Article II covered tropical peat swamp forests and fens. These sites are the Peruvian Amazon, French Guiana, Uganda, Burma, and the Malaysian Borneo states of Sarawak and Sabah. This was done to see if the tropical hot climate exhibited different patterns of peatland GHG exchange regionally compared to global peatlands (Article I). Field sampling was conducted during both the dry season (i.e. annual water table minimum) and rainy period (annual water table maximum) of each site between 2013 and 2022. Study sites represent peatlands that have been arable for >5 years (Borneo, Burma, Peru and Uganda), intensively (more than once a year) grazed peat meadows (Uganda), and drained fens (French Guiana and Burma), swamp forests (Peru, Sabah and Sarawak) and fens under no direct human influence in each study region. The field sampling scheme, data analysis methods, and GPP data are the same as in Article I. Here, I tested if the GHG exchange, (specifically N_2O and CO_2 fluxes) differed in their response to variations observed in SWC.

2.2. Impact of climate change and extreme drought on carbon cycle (Articles III & IV)

Following the analysis of the implications of SWC on GHG exchange in global open peatlands, I investigated the soil–plant–atmosphere exchange of CO_2 and its micro-meteorological drivers in a flooded sub-Arctic fen peatland (Article III) and its coupling with water cycle under atmospheric drought (Article IV). In Article IV, I further explored plant physiological responses to the drought. While article I and II systematically covered global open peatlands, drought and climate change impacts on peatlands were not explicitly tested. Furthermore, Articles I and II did not have the temporal dynamics (focused on growing season fluxes) required to provide unequivocal evidence on the direct and indirect effects of climate change and mechanistic understanding of the SWC variability and its implications on GPP. I filled these knowledge-gaps in article III and IV. I selected a high latitude fen site (Bonanza Creek rich fen, Alaska, USA; Article III) and a temperate bog site (Burns Bog, Vancouver, Canada; Article IV) with publicly available EC data. Bonanza Creek was selected to test the impact of high latitude warming on C cycle and SWC. Burns Bog was selected as it was impacted by prolonged atmospheric drought. While Bonanza Creek was flooded (60 cm above the surface) during most of the study period (7 years), Burns Bog remained above 80% SWC across the five-year period. Two distinct approaches were used to investigate these processes.

2.2.1. High latitude warming and C cycle (Article III)

In Article III, I used a Bayesian model-data fusion framework (MDF) framework, CARDAMOM, that calibrates DALEC2 (intermediate complexity terrestrial ecosystem model of C) at the site scale using site-specific biophysical and biogeochemical observations (outlined below). I examined the meteorological and biophysical factors that govern the IAV of CO_2 fluxes and plant C traits describing internal dynamics such as photosynthate allocation to different plant tissues, residence time of C in the live and dead biomass pools by considering a seven-year weekly time step (2014–2020). For this, I initialised the model with in-situ observations of SOC), aboveground biomass (AGB), and fine root carbon (FRC) stock. The model was calibrated with a publicly available EC tower dataset (US-BZF; Euskirchen, 2022a) and earth observation (EO) data. I used the model retrieved C variables (NEE, GPP, Reco, and leaf area index (LAI)) to investigate the reasons behind the IAV of plant C dynamics and C uptake at the site scale. Additional synthetic experiments on the calibrated model were carried out to examine the individual effects of the climatic drivers on the IAV of GPP, LAI and R_h. A generic overview of the analytic steps I took is summarised in Figure 4. The study site, model inputs, model, Bayesian framework, synthetic experiments, and statistical tests performed are outlined below.

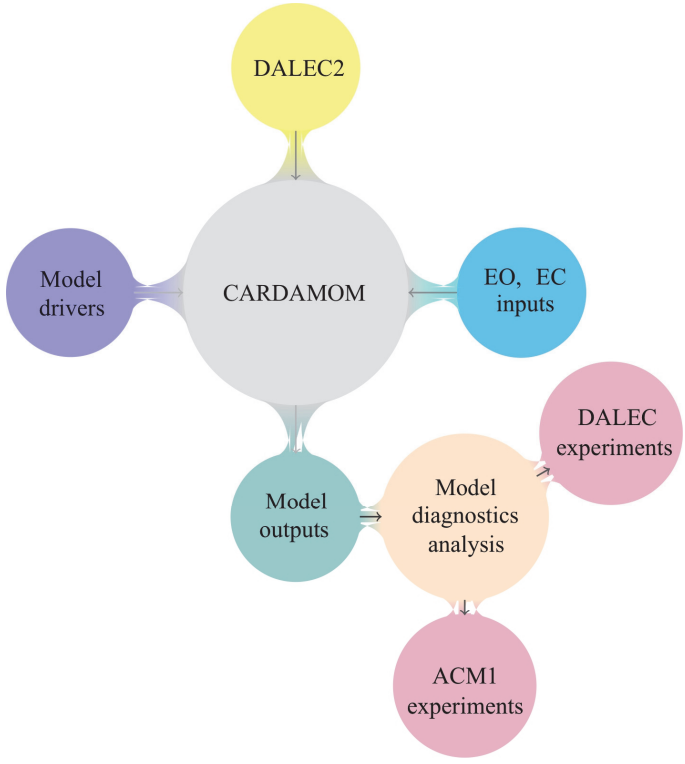

Figure 4: Model–data fusion methodology

Model site: Bonanza Creek

Bonanza Creek is a rich fen peatland situated ~45 km south-east of Fairbanks in interior Alaska (64.82°N, 147.87°W). The site is positioned in the Tanana River floodplain and is characterised as rich fen (pH 5.2 to 5.4). The vegetation is comprised of marsh cinquefoil (*Potentilla palustris*), wheat sedge (*Carex atherodes*), water horsetail (*Equisetum fluviatile*), and ground cover mostly comprised of brown mosses (*Drepanocladus aduncus* and *Hamatocaulis vernicosus*) and sparse *Sphagnum spp*. (Euskirchen et al., 2020). The site is part of a long-term ecological experimental study. Aboveground carbon (AGC) stock for the year 2009 was 282 (standard error (SE): ± 49.165) g C m^{-2}. Ancillary aboveground NPP of 186.5 (63.16) g C m^{-2} y^{-1} and a maximum vascular green area of around 2.5 m^2 m^{-2}, achieved in the summer season. The peat depth is ~1 m and is within an area of discontinuous permafrost with seasonal freezing. The long term (1917 to 2000) mean annual temperature is –3.1°C. The mean annual air temperature for 2014 to 2020 was –0.95°C. Following the updated Köppen climate classification scheme, the site falls within the sub-Arctic climate (continental, warm summer, without a dry season; Dfc zone) (Kottek et al., 2006).

Model inputs

I used observations spanning in-situ inventory, EC, EO and database information. NEE and night-time partitioned Reco (Reichstein et al., 2005) were extracted from EC (US-BZF, Euskirchen, 2022a). I chose night-time partition modelled data over day-time partition because it aligns with the in-situ GPP (Churchill et al., 2015; Fan et al., 2013). Uncertainty associated with NEE was assumed to be 0.58 g C m^{-2} day^{-1} based on an analysis by Hill et al., (2012) and previously applied in CARDAMOM (e.g. Famiglietti et al., 2021). Reco uncertainty is composed of the NEE uncertainty and the mean mass balance mismatch from the flux partitioning (0.16 g C m^{-2} day^{-1}) and inflated to account for uncertainty in the partitioning approach totalling an uncertainty of 1 g C m^{-2} day^{-1}. Time series information on LAI was extracted from the 300 m Copernicus product Fuster et al., (2020), using the product provided SE but with a minimum bound of 0.5 m^2 m^{-2} to account for model-structural uncertainty. Continuous LAI time series were only available for the months starting from April until September for most of the seven years, while the rest were absent because of the deciduous nature of the plant foliage. MDF does not require gap-filled data. Each input must have associated uncertainty. MDF is capable of estimating parameter ensembles and steady state. The data gaps are accounted for in the uncertainty characterisation. This is one of the several advantages of MDF in comparison with traditional process-based and statistical models. I assimilated NEE, LAI, at weekly time step. The in-situ SOC stock and fine root C stock were used to initialise the model. AGC stock data was assimilated as a time series, and it was used as a point in the first week of 2014, leaving the rest of the time steps empty. I assimilated EC and LAI data from the alternating years (2014, 2016, 2018, 2020). The remaining EC and in-situ data were used for model validation (see Table 1 for the list of in-situ data).

Table 1: In-situ measurements used for the model calibration and validation with CARDAMOM. *assimilated data

Parameter	Value ± SE	Unit	Relevant literature
Total NPP	214.33 ± 150.5	g C m^{-2} y^{-1}	Churchill et al. (2015)
BG NPP	34.8 ± 10.16	g C m^{-2} y^{-1}	Churchill et al. (2015)
AG NPP	186.5 ± 63.16	g C m^{-2} y^{-1}	Churchill et al. (2015)
AGC*	282 ± 49.16	g C m^{-2}	Churchill et al. (2015)
FRC*	247.06 ± 140.86	g C m^{-2}	McConnell et al. (2013)
SOC*	64055 ± 5000	g C m^{-2}	Fan et al. (2013)

Model drivers

Weekly time step meteorological data (Table 2) were required as model drivers. I used the atmospheric CO_2 concentration for 2014, 2015 and the first six months of 2016 from the nearby black spruce forest EC data (US-BZS, (Euskirchen, 2022b), because the measurements for this period were unavailable for the rich fen peatland.

Table 2: Meteorological drivers for the model calibration

Drivers	Unit
DOY	Day of year
Minimum temperature	°C
Maximum temperature	°C
Mean temperature	°C
Incoming shortwave radiation Atmospheric CO_2 concentration	MJ m^{-2} day^{-1} ppm
Precipitation	mm day^{-1}

Model: DALEC2

DALEC2 is a C mass balance model representing four live and two dead biomass pools (Figure 5). Parameters within DALEC2 represent the initial C states in the first time step and define the internal C cycling and their sensitivity to the environment (Table 3). I conducted an exhaustive meta-analysis on the CO_2 dynamics (focusing on internal C traits) of northern peatlands and other high-latitude ecosystems, including the Arctic tundra. Key findings are summarised in the supplementary file of Article III. Using the results of the meta-analysis I updated prior estimates on parameters describing the fine root turnover and initial C stocks of fine root and aboveground pools (Table 3). The meta-analysis findings were also used as a measure of validation in addition to the validation with EC tower data. Additionally, I updated the default R_a:GPP ratio (= plant carbon use efficiency (CUE)) to an initial prior estimate of 0.62 (Collalti et al., 2020; Hermle et al., 2010). I also changed the initial prior canopy efficiency value to 16.9 g C m^{-2} day^{-1} with a SE of 7.5 g C m^{-2} day^{-1} (derived from the TRY database Kattge et al., 2011). The rest of the uniform prior parameter ranges used in the model were left as default (Bloom & Williams, 2015). R_a is estimated as a time invariant but parameterisable for each location independently fraction of GPP, the remainder being NPP. NPP is then allocated to the four live biomass pools using fixed fractions retrieved during the calibration process. Canopy growth is determined by a combination of direct allocation of NPP and C supply from a labile pool based on a day-of-year model. Canopy senescence in a litter pool is determined by a day-of-year model. The litter pool is either decomposed

to SOC or released as R_h based on an exponential temperature function. Mineralisation of SOC also follows an exponential temperature function.

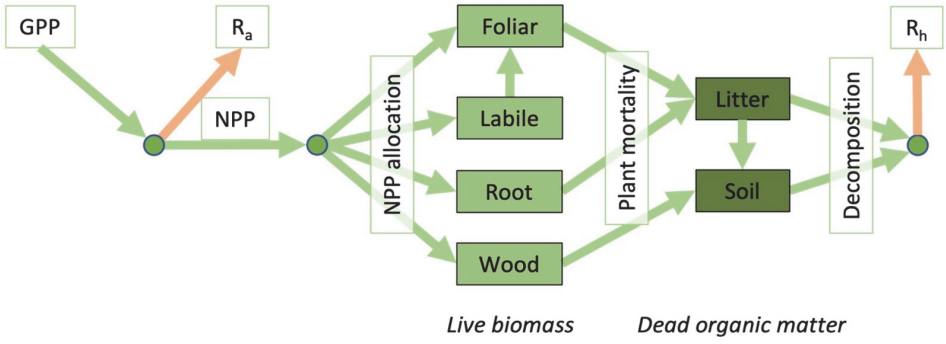

Figure 5: DALEC2 C path

Table 3: DALEC2 parameters and initial C pool stocks

No	Description	Prior range	Unit
P(1)	Decomposition of litter to SOM	0.00001– 0.01	Fraction
P(2)	Autotrophic respiration fraction	0.2–0.8	Fraction
P(3)	Fraction of GPP allocated to foliage C pool	0.01–0.5	Fraction
P(4)	Fraction of GPP allocated to fine roots	0.1–0.8	Fraction
P(5)	Leaf lifespan	1.001–6	Years
P(6)	Woody C turnover rate	0.000009–0.001	Fraction/day
P(7)	Fine root C turnover rate	0.0008–0.0004	Fraction/day
P(8)	Litter C turnover rate	0.0001141–0.02	Fraction/day
P(9)	Soil organic C turnover rate	10^{-7}–10^{-3}	Fraction/day
P(10)	Temperature dependence exponent factor	0.019–0.08	unitless
P(11)	Photosynthetic canopy efficiency	1.64–42	g C m^{-2} day^{-1}
P(12)	Maximal bud burst day	1–365.25	day of year
P(13)	Fraction of GPP allocated to labile	0.01–0.5	Fraction
P(14)	Labile release period	10–100	days
P(15)	Maximal leaf fall day	1–365.24	days
P(16)	Leaf fall period	20–150	days
P(17)	Leaf C per area	20–180	g C m^{-2}
P(18)	Labile C pool at initial time	1–2000	g C m^{-2}
P(19)	Foliar C pool at time t	1–2000	g C m^{-2}
P(20)	Fine root C pool at time t	1–750	g C m^{-2}
P(21)	Above and below woody carbon pool at time t	1–400	g C m^{-2}
P(22)	Litter C pool at time t	1–2000	g C m^{-2}
P(23)	Soil organic C pool at time t	200–125,000	g C m^{-2}

No	Description	Prior range	Unit
P(24)	Resilience factor burned but not combusted C stocks	0.1–1	Fraction
P(25)	Foliage Combustion completeness factor	0.01–0.99	Fraction
P(26)	Fine root and wood combustion completeness factor	0.01–0.99	Fraction
P(27)	Soil combustion completeness factor	0.001–0.1	Fraction
P(28)	Foliage and fine root litter Combustion completeness factor	0.01–0.99	Fraction

Bayesian model–data fusion framework: CARDAMOM

The CARDAMOM MDF framework uses a Bayesian approach within an adaptive proposal Markov chain Monte Carlo algorithm (Haario et al., 2001) to retrieve ensembles of model parameters and pool sizes (28 parameters; Table 3) for a model that is consistent with the observations, their uncertainties and ecological theory embedded in ecological and dynamical constraints (EDC) (Bloom & Williams, 2015). The use of a Markov chain Monte Carlo algorithm allows uncertainty characterisation without assuming the shapes of the distribution. The Markov chain Monte Carlo algorithm, with the help of EDCs, uniform prior ranges (Table 3), and initial prior estimates (where applicable), retrieve a sample parameter hyperspace. This then becomes the new prior estimate, which is then tested against the assimilated data and draws new sets of parameters that are consistent with EDCs, and the other samples are rejected. CARDAMOM analyses each time step three times (known as chains) independently and assesses 100 million parameter proposals in each chain. 100 subsamples (parameter ensembles) are drawn from each of the three chains to estimate the posterior probability density for each of the 28 parameters. The retrieved parameter ensembles allow us to directly quantify parameter uncertainty and, through simulating these ensembles, the uncertainty in the ecosystem C stocks and fluxes. The likelihood estimates of the posterior parameter probability estimates generated by CARDAMOM were normalised by calculating square root to balance multiple data constraints and the imbalance between a large volume of EC data compared to the field observations (Wutzler & Carvalhais, 2014).

Model diagnostic analyses

CARDAMOM calibrated weekly time step posterior probability distributions of C variables, meteorological drivers, and time-invariant parameters along with their characterised uncertainties at 95% confidence interval (CI) (it is estimated using quantiles (in fractional form); 0.025, 0.5 and 0.975) was averaged at an annual scale. To assess the associations between fluxes, parameters, and climatic factors, we calculated the changes in CARDAMOM profiled probability estimates of C fluxes relative to the year 2014 to find the driving factors behind the

growth in production in the ecosystem. Further corroborative analysis using simple linear regressions to answer the research questions was also conducted.

Two simulation experiments on the calibrated DALEC were designed to extract information on the independent contribution of the meteorological drivers in CO_2 exchange. To do this, the retrieval of the C variables at a fixed atmospheric CO_2 concentration (400.584 ppm; this estimate represents the atmospheric CO_2 concentration on the first week of the study period, simulated DALEC and calculated C variables) was repeated. This was then compared with the original CARDAMOM-calibrated DALEC estimates. These original CO_2 estimates (from the sensor onboard the EC tower), on average, were increasing during the study period (mean annual estimate is 432 ppm). In the second experiment, the IAV in the meteorological drivers were removed (except atmospheric CO_2 concentration) by aggregating at weekly time steps and estimated the mean across the seven-year study period (estimated mean of week 1 for each year, week 2 for each year and so on). The retrieval of the C variables was repeated and compared against the CARDAMOM profiled DALEC estimates.

Next, the direct CO_2 fertilisation effect and the indirect effect through the changes in LAI were isolated by driving ACM-1 with the respective model drivers of the two experiments. The difference in ACM-1 estimated GPP and the respective experiments represent this indirect effect. Finally, I inferred on the role of SWC on GPP and NEE by checking the correlations between weekly time step estimates at annual scale, specifically for growing season and for the data in its entirety.

2.2.2. Atmospheric drought and water–carbon coupling (Article IV)

As briefly mentioned above, I investigated the impact of atmospheric drought and SWC drawback on GPP. Specifically, I did an ecosystem scale diagnostic analysis of the physiological and aerodynamic constrains on water transport in the soil- plant-atmosphere continuum. I then estimated the consequent temporal variability of environmental controls on GPP using an approach called empirical dynamic modelling (EDM) (Sugihara et al., 2012). The EDM was used to retrieve the time-varying causal links between GPP and its meteorological drivers in Burns Bog, Vancouver, Canada (detailed below). The model was driven by leveraging the publicly available EC dataset (CA-DBB; Christen & Knox, 2022) and in-situ observations from the weekly time step for five years from 2016 to 2020.

Burns Bog

The CA-DBB EC station is located in Burns Bog, City of Delta, British Columbia, Canada (49.129°N, 122.986°W). Burns Bog is a degraded ombrotrophic peat bog in the Fraser River Delta. Peat was harvested in the bog between 1930 and 1970. It has since been reduced to approximately 58% of its original size through drainage, harvesting, and encroachment of agricultural and industrial lands. The bog was formally protected with the establishment of the Burns Bog

Ecological Conservancy Area in 2001. Re-wetting via ditch blocking began in 2007 to raise the water table and promote peat development. The climate of Burns Bog is characterized by warm dry summers and mild wet winters (Köppen climate classification scheme; Csb, Kottek et al., 2006). The climate norm (1990–2020) from nearby Vancouver International Airport indicates the area receives peak precipitation between November and January (> 170 mm / month), while drought conditions are common in July and August (< 40 mm / month). In the winter, water flows radially from the centre to the edges of the bog, while in the summer, there is minimal lateral flow. Vegetation in Burns Bog is diverse, the area around the CA-DBB EC station dominated by *Sphagnum spp*. moss and white beak sedge (*Rhynchospora alba*).

Atmospheric drought detection

Atmospheric drought was determined by combination of standard precipitation evapotranspiration index (SPEI) (Beguería et al., 2014; Vicente-Serrano et al., 2010a; Vicente-Serrano et al., 2010b) and moisture coefficient (MC) (Pereira et al., 2015). First, MC was estimated as the ratio of ET to potential evapotranspiration (PET) (eq. 2.5). Weeks with a value below 0.6 were considered as plant water stressed (Allen et al., 1998).

$$MC = \frac{ET}{PET} \tag{2.5}$$

where PET is the water that would have evaporated and transpired if the ecosystem had enough water. PET was estimated using the Penman method (Penman, 1948) (eq. 2.6). The Penman equation calculates daily potential evaporation that combines an energy equation based on net incoming radiation with an aerodynamic approach.

$$PET = \frac{s}{s+\gamma} \times \frac{R_n}{\lambda} + \frac{\lambda}{s+\lambda} \times E_a \tag{2.6}$$

where PET is the daily potential evapotranspiration (in mm day^{-1}) from a saturated surface (aggregated by weeks for compatibility with the rest of the data), R_n is the daily incidental short-wave radiation to the evaporating surface (in MJ m^{-2} day^{-1}), s is the slope of the saturation vapour pressure curve kPa °C^{-1}) at a given air temperature, γ is the psychrometric constant (kPa °C^{-1}), and λ is the latent heat of vaporization (in MJ kg^{-1}). E_a (in mm day^{-1}) is a function of the average daily wind speed (u, in m s^{-1}), and VPD (D, in kPa):

$$E_a = f(u) \times D = f(u) \times (v_a^* - v_a) \tag{2.7}$$

Where v_a^* is the saturation vapour pressure (kPa). $v_a$is the actual vapour pressure (kPa). $f(u)$ (Eq. 2.8) is a function of wind speed (Penman 1956):

$$f(u) = 2.626 + 1.381 \times u \quad (2.8)$$

Finally, the SPEI was calculated using the R programming environment (R 4.1.3) package SPEI (version 1.8.1). SPEI compares the highest PET to current water availability. See Beguería et al., (2014) and Vicente-Serrano et al., (2010a, b) for more details.

Water transport through the soil–plant–atmosphere continuum

The bulk surface conductance (G_{sw}) (m s^{-1}), eq. 2.9)) to latent heat transfer was estimated by inverting the Penman–Monteith model for evapotranspiration (Knauer et al., 2018). Here, the vegetation is represented as a single uniform layer / one large canopy (i.e. 'big leaf'). The model estimates the combined conductance of the soil and plant surface. G_{sw} was estimated at weekly time step using the EC data.

$$G_{sw} = \frac{\lambda \times E \times G_{ah} \times \gamma}{s \times (H + \lambda \times E) + \rho \times c_p \times G_{ah} \times D - \lambda \times E \times (s + \gamma)} \quad (2.9)$$

where G_{ah} (eq 2.10) is the bulk aerodynamic conductance for heat transfer (m s^{-1}). E is the evaporation rate or flux of water vapour.

$$G_{ah} = (R_{am} + R_{bh})^{-1} \quad (2.10)$$

R_{am} is the aerodynamic resistance to momentum transfer (or $1/G_{am}$, where G_{am} is the aerodynamic conductance; Eq. 2.12) with turbulence as the principal transport mechanism. R_{bh} is the canopy (quasi-laminar) boundary layer resistance ("excess resistance") to heat transfer (or $1/G_{bh}$, where G_{bh} is the quasi-laminar boundary layer conductance) (Massman, 1999; Verma, 1989). I calculated G_{bh} as a function (eq. 2.11) of friction velocity (u_*, m s^{-1}) following Thom, (1972).

$$G_{bh} = (6.2 \times {u_*}^{-0.67})^{-1} \quad (2.11)$$

G_{am} is a function of u_* and wind speed (m s^{-1}) (eq 2.12)

$$G_{am} = \frac{{u_*}^2}{u \times (z_r)} \quad (2.12)$$

The analysis outcomes were used to study the intra-annual changes in G_{sw} in the Burns Bog peatland. Next, evaporative fraction (EF) was calculated (eq 2.13) to understand how much of the available energy was used for ET from the peat surface. The relationship of EF with SWC and G_{sw} were also plotted.

$$EF = \frac{\lambda \times E}{\lambda \times E + H} \quad (2.13)$$

Causation from time series data (empirical dynamic model)

In this study, a causal inference approach was used to study the causation between GPP and its drivers. EDM is an equation-free mechanistic model framework (Deyle et al., 2016; Deyle & Sugihara, 2011; Sugihara et al., 2012; Ye et al., 2015) centred around state space reconstruction (Deyle & Sugihara, 2011; Kugiumtzis, 1996; Vlachos & Kugiumtzis, 2009). It applies to complex dynamic systems where the relationships between the interacting variables vary with changes in the system state (Sugihara et al., 2012; Ye et al., 2015) and cannot be described by equations and the hypotheses and assumptions that come with it. EDM is thus only constrained by the amount and the quality of the data. The purpose of using EDM in this study was twofold: (a) to study the interactions between variables and (b) to detect causation.

I used convergent cross mapping (CCM) to extract causation from the time series data (R package rEDM; Version: 1.14.0; function: ccm). At the heart of the CCM is its ability to detect and separate causation from spurious correlations in time series data of complex coupled dynamic systems. The analysis is based on the theory put forward by Takens, (1980), which states that in a multidimensional dynamical system with only a finite number of observable variables, the essential information of the system is retained in the time series of any observed single variable of that system. This means we can replicate the system dynamics by using the lagged time series of the observable variable in place of the unknowns. Thus, if causation exists between two variables, it can be extracted from the time series history of the affected variable (cross-mapping). The effectiveness is then cross map skill was reported (ρ). I examined the variation in causality between GPP and factors such as Tair, ET, VPD, atmospheric CO_2 concentration, SWR, SWC, and WTD across the five-year study period (259 weeks together) and for each year with a time lag of 1 week by applying CCM (Sugihara et al., 2012). ρ, of each pair (GPP:ET, GPP:Tair and so on) was reported. SE of ρ was estimated by the equation below (eq 2.14) (Gnambs, 2023).

$$SE = \frac{1-\rho^2}{\sqrt{N-3}} \tag{2.14}$$

I used redundancy analysis (RDA) on the five-year data (R package: vegan version 2.6-4; Oksanen et al., 2001) to extract the direction and magnitude (length of the arrows) of causal strength estimates from above, along with SWC, WTD, Tair, VPD, ET, SWR, and atmospheric CO_2 concentration. Furthermore, a random forest regression was performed (*randomforest* R package) on the factors used in the RDA, and then relative variable importance (relative to the most significant variable for estimating GPP) was calculated for predicting GPP. The adjusted R^2 and corresponding p values of the random forest regression were reported. I also performed a cross correlation between ET and SWC using the weekly estimates. The cross-correlation test assessed the lag between ET and the decrease in SWC. A 95% CI and the significance were assessed based on the p-value.

3. RESULTS

3.1. Soil moisture and GHG exchange (Articles I, II, III & IV)

3.1.1. GHG exchange across the soil moisture spectrum (Article I and II)

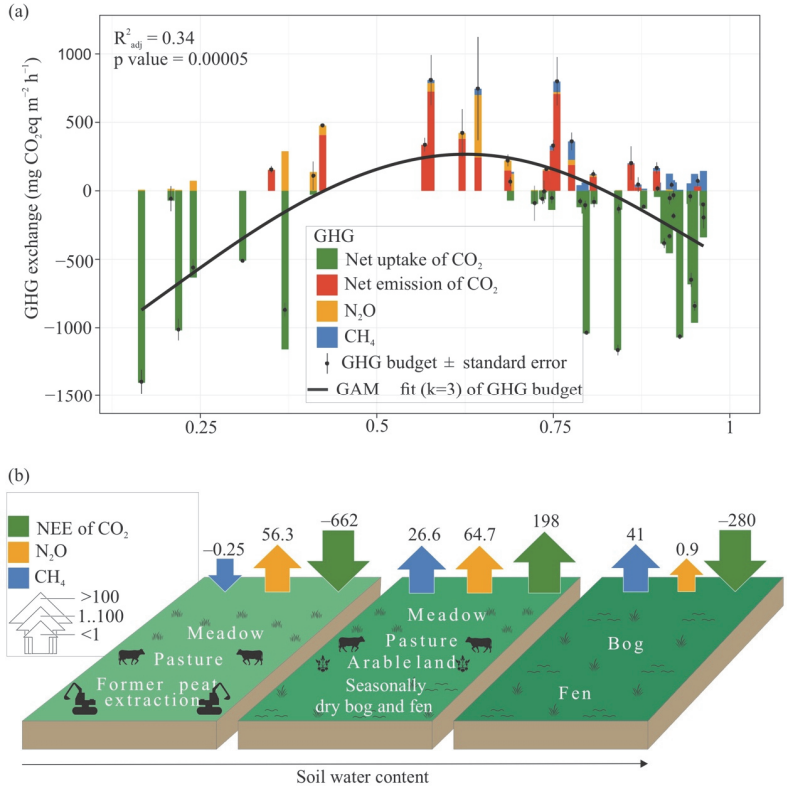

Figure 6: GHG exchange in 48 open peatlands along the SWC gradient. **a:** Green bars represent net uptake of CO_2. Red bars represent net emission of CO_2. Blue bars represent the CH_4 fluxes. Orange bars indicate N_2O fluxes. All fluxes are site averages in mg CO_2eq m^{-2} h^{-1}. The black convex line is the GAM fit at k =3 for the 48 site average values of GHG. Error bars are respective SE estimates. **b:** Schematic breakdown of GHG exchange in each land use covered in this study. (Source: Article I).

CO_2 dominated the GHG exchange in both the net emission (>100 mg CO_2eq m^{-2} h^{-1}) and uptake (< –100 mgCO_2eq m^{-2} h^{-1}) (Figure 6) across open peatlands globally. On the other hand, in the tropics, while CO_2 dominated the GHG uptake (−160 mg CO_2 m^{-2} h^{-1}) as seen globally, N_2O was the prevalent flux in emissions (90 mg CO_2eq m^{-2} h^{-1}). N_2O emissions were mostly from moderately wet peatlands (SWC: 0.35 to 0.7 m^3 m^{-3}). Consequently, CO_2 removal offsets emissions of N_2O and CH_4 emissions in the high GHG sink ecosystems. In the high GHG

source sites, the net emission of CO_2 contributed >83% of each GHG exchange. The GHG-neutral sites (between −100 and +100 mg CO_2eq m^{-2} h^{-1}) experienced modest fluxes of all three GHG (Figure 6).

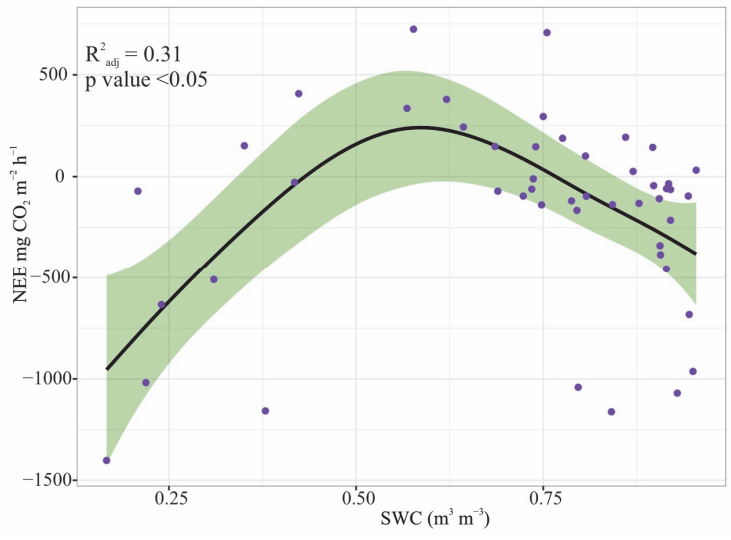

Figure 7: Univariate GAM model of NEE with SWC. Negatives are sinks and positives are emissions

Articles I and II found an optimum of GHG and CO_2 exchange (emissions) across the soil moisture gradient for global and tropical peatlands. The net GHG (GAM model fit: R^2_{adj} = 0.34) and NEE (R^2_{adj} = 0.31) emissions were peaked at intermediate SWC (i.e. 0.4 m^3 m^{-3} to 0.75 m^3 m^{-3}) (Figure 7). This finding opposes the notion of a universal positive relationship of soil moisture gradient with GHG and NEE changes. Here, the dry sites were also net sinks of GHG and NEE.

3.1.2. Soil moisture and GPP in the warming sub-Arctic (Article III)

SWC in Bonanza Creek did not exhibit a Gaussian response which contradicts the findings of Article I and II. Several factors contribute to this difference. Initially, Articles I and II analysed data spanning over 48 open peatlands. These covered extremely dry, moderately moist and wet sites across different climates and land uses. Secondly, each site covered growing season data of 4 to 6 days. Finally, Articles III and IV are single site ecosystem scale analysis of years of data at weekly time step which captured seasonal variations. Moreover, Bonanza Creek (Article III) was flooded (>60 cm from the peat surface) for most growing seasons (2014–2020). At annual scale, soil moisture explained ~60% of the variability in GPP (Figure 8c; R^2 = 0.59, F-statistic = 9.27 on 1 and 5 degrees of freedom, p-value = 0.05) with a positive linear trend (Evans et al., 2021). This can be caused by the saturated conditions of growing seasons as they were

skewed from the winter-frozen dry readings in the annual average. Weekly estimates of SWC did not explain any variations in GPP (Figure 8a) and NEE (Figure 8d). The growing season data across the seven years provide similar accounts as well (Figure 8b, e). All growing season variation in SWC (Figure 8a, b) happens during saturated conditions. Similarly, Laine et al., (2019) showed that the water table did not have any impact on primary production in a sub-arctic Finnish fen. However, these estimates might not be a realistic representation of the site conditions since it was flooded. Analogous outcomes were reported for leaf production in a bog and poor fen in southern Finland (Köster et al., 2023). During periods of inundation, algal production has been reported to contribute significantly to GPP. Algal contribution during periods of inundation is found at drier sites rather than those with constant inundation (DeColibus et al., 2017; Wyatt et al., 2012), especially in previously drier sites as opposed to sites with constant inundation (Kane et al., 2021). Hence it is likely that GPP was influenced by algal production during the flood years of 2014, 2016, 2017 and 2018. This might have contributed to the underestimation of CARDAMOM simulated GPP compared to night-time partition EC data. For the aforementioned reason, DALEC did not include soil moisture input and parameterisation.

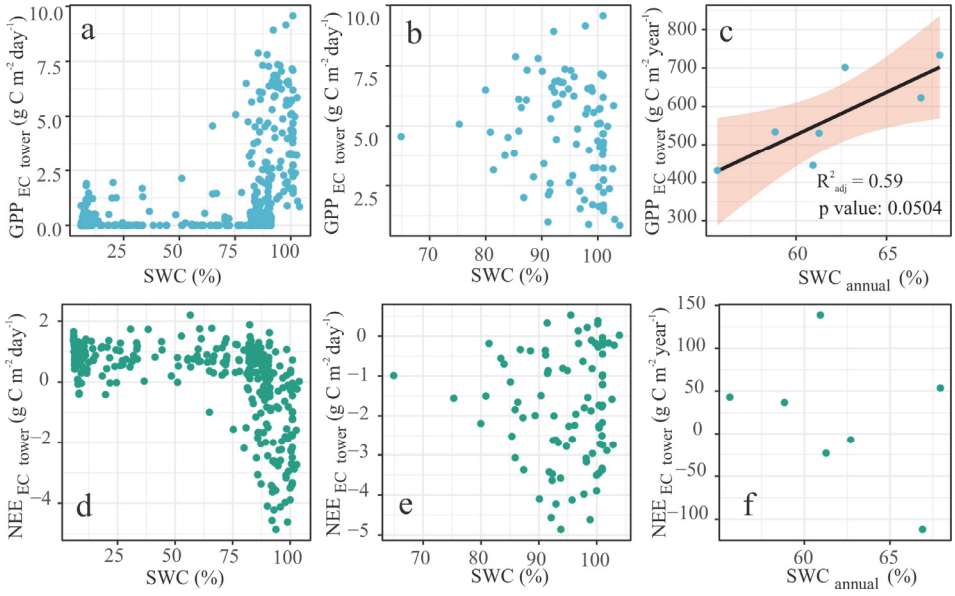

Figure 8: SWC does not explain variations in NEE and GPP. **a**: at weekly time- step for all seasons, **b** growing season, **c**: mean annual scale plotted against SWC. **d**, **e**, and **f** depict the relationship of NEE with SWC in the same temporal order as GPP (Source: Article III).

3.1.3. Water in the soil–plant–atmosphere continuum (Article IV)

Burns Bog preferred water retention over C assimilation due to atmospheric aridity during the five-year study period. This finding contradicts Articles I, II and III. In 2016, the drought was severe (Table 4). Following criteria were considered to classify the parameters into high and low years in Burns Bog. The plant–water stress is considered relatively high if the fraction is below 0.4. Similarly, a drought is considered severe when SPEI is –1.5. G_{sw} and ET were classified as high for years with G_{sw} 0.2 m s^{-1} and ET 3 kg H_2O m^{-2} day^{-1}. SWC drawdown is considered high when it falls below 82.5%. EF is considered high when it is above 0.5.

Table 4: Annual variability of drought-related parameters (Source: Article IV).

Unit		High (Years)	Low (Years)
M.C	Fraction	2016, 2019	2017, 2018, 2020
Drought	Fraction	2016, 2020	2017, 2018, 2019
G_{sw}	m s^{-1}	2017, 2018	2016, 2019, 2020
ET	kg H_2O m^{-2} day^{-1}	2017, 2018	2019, 2020
SWC	%	2017, 2018	2016, 2019, 2020
EF	Fraction	2016, 2017, 2018	2019, 2020

Nevertheless, the ecosystem did not transpire a proportionate amount of water due to stomatal regulation (Table 4); low rates of ET and increased EF in 2016 imply high soil evaporation rates and low transpiration rates. In the subsequent years (2017 and 2018), a reduction in plant-water stress – evidenced by high G_{sw}) and elevated EF, indicating minimal stomatal regulation (Figure 9a, Table 4) was attributed to decreased drought severity (Table 4). This reduction in stress led to higher ET rates, reaching 3 kg H_2O m^{-2} day^{-1} (Figure 9b, Table 4). GPP was thus highest in 2018 (~3.2 g C m^{-2} day^{-1}). The relative increase in ET caused surface water drawback during the winter months of 2017 and 2018 (82.5% and 80% of the field capacity). Consequently, the water table depth dropped to –8cm. However, the drawback had ~14 week lagged response to ET (correlation coefficient of 0.77 ($p < 0.001$) at a 95% CI and 257 degrees of freedom, Figure 9b). EF experienced a decline, and the ecosystem experienced water stress. Contrary to 2016, 2019 water stress was thus caused by the surface drying out (SWC below 82.5% field capacity (Figure 9b) and WTD of –8cm or below. As the SWC dropped below the threshold of 82.5% (WTD of –8 cm), G_{sw} (Figure 9c) and ET (Figure 9b, Table 4) declined (1.8 kg H_2O m^{-2} day^{-1}). Thus, GPP was only 2.5 g C m^{-2} day^{-1} (Figure 9d). Interestingly, SWC dropped only to 85% during the dormancy season of 2019 (Figure 9b). 2020 saw a severe drought, and the fluxes dropped similarly to the 2016 drought (Figure 9). However, the plant water stress was not as high as in 2019. Also, while GPP generally exceeded Reco during the study period (Figure 9, Satriawan et al., 2023), the site became a net source of C to the atmosphere (11.9 ± 15.1 g C m^{-2} $year^{-1}$) by 2020 (Satriawan et al., 2023).

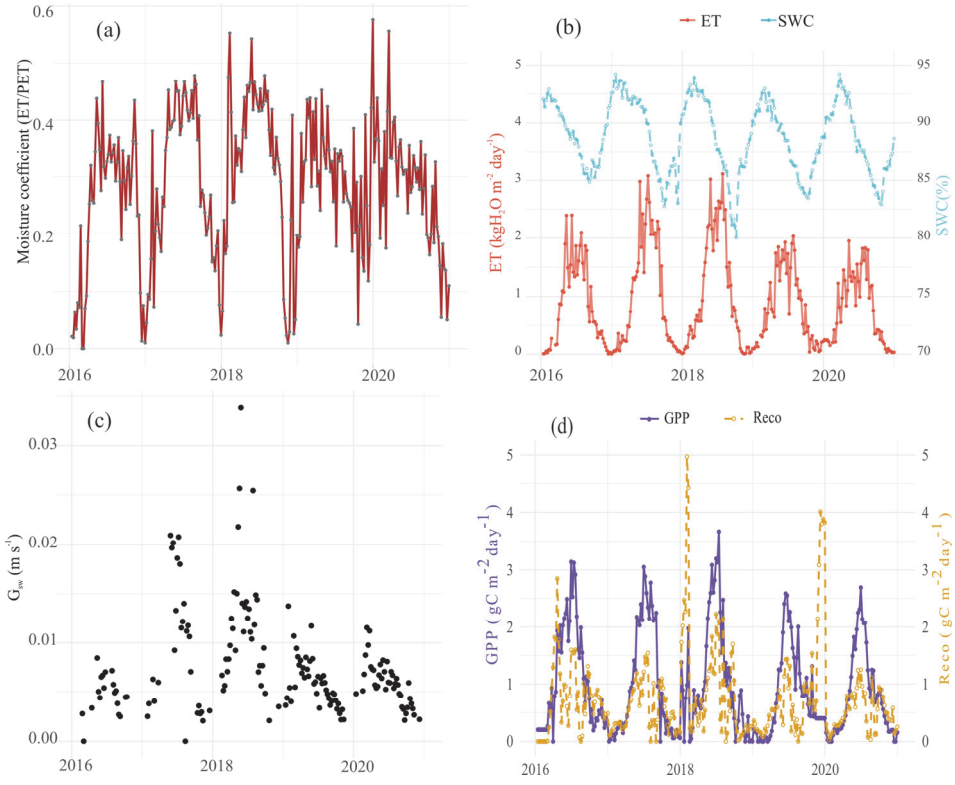

Figure 9: Weekly time step water and carbon dynamics at Burns Bog for five years from 2016 to 2020. **a**: The moisture coefficient shows the variability in the severity of the atmospheric drought. **b**: temporal variability in SWC (blue dashed lines) and ET (orange lines). **c**: intra-annual variability in G_{sw}, and finally **d**: variability in GPP (purple lines) and Reco (orange dashed lines). (Source: Article IV)

3.1.4. Causal relationships for 2016 to 2020 (Article IV)

GPP was regulated by energy-related factors when the entire weekly time step data for five years were considered (Figure 10). A strong coupling was observed between GPP and ET and VPD (Figure 10b). The effect of ET on GPP (ET:GPP) was stronger (0.65 ± 0.03) than the impact of VPD (VPD:GPP; 0.59 ± 0.04) and SWR (VPD:SWR; 0.58 ± 0.04) on GPP. The effect of GPP (feedback) on these variables (GPP:ET and GPP:VPD) was equally strong (0.58 ± 0.04 and 0.52 ± 0.04, respectively). CCM revealed a significant impact of SWC and WTD on GPP (Figure 10b). This was also evident from the temporal variability of plant physiological properties (Figure 9c). On the other hand, these findings differ from the correlation analysis (Figure 9a). We also found that the impact of SWC on VPD (SWC:VPD) (0.57 ± 0.04) was greater than its effect on GPP (Figure 10b). However, this was weaker than the effect of ET:GPP, VPD:GPP, and Tair:GPP (Figure 10b). ET and Tair exhibited a strong causal link and so did ET and VPD. However, climate–carbon feedbacks between atmospheric CO_2 concentration

and GPP were insignificant in this five-year dataset. This is because the CO_2 concentrations did not increase over the period.

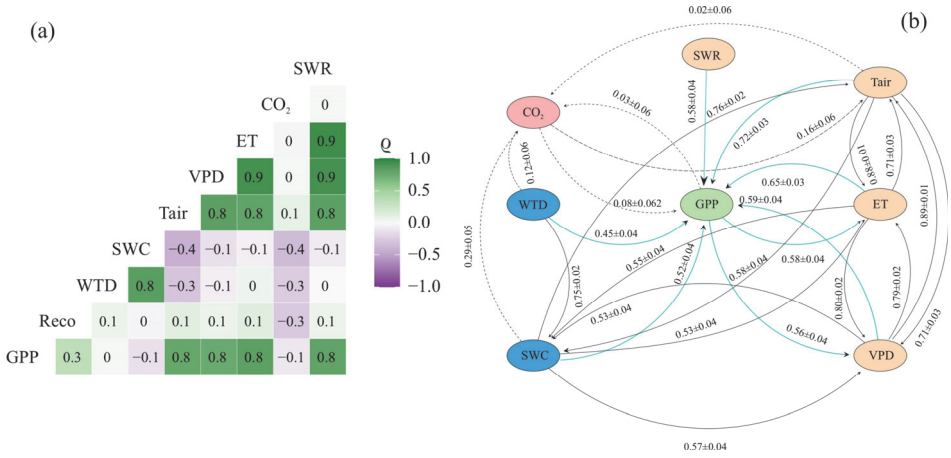

Figure 10: Statistical regression and causal inference of weekly time step data for 2016 to 2020. **a**: correlation matrix using the Pearson correlation coefficient. **b**: multivariate causation cross-map skills retrieved using the CCM analysis. The cross-map skill is displayed using the Pearson correlation coefficient (ρ). The black dotted lines indicate weaker causal relationships. The coloured lines show the direct causal relationships between GPP and SWR, VPD, Tair, SWC, WTD, ET, or atmospheric CO_2 concentration (indicated as CO_2). The black solid lines indicate causation between variables. (Source: Article IV)

3.1.5. Temporal variability of energy and water limitation of GPP (Article IV)

Causal inference of individual years showed temporal variability of energy and water limitation of GPP. Results were in commensurate with water movement in the soil-plant-atmosphere continuum. Causal inference (CCM) found 2016, 2017, and 2018 GPP to be energy limited (Figure 11). Energy limitation is driven by a stronger causal effect of SWR, Tair, VPD, and ET relative to SWC or WTD (Figure 11a). Observed energy limitation is consistent with stomatal regulation during the 2016 drought and subsequent high rates of ET (2017, and 2018) (Table 4, Figure 9b, c and d). In contrast, GPP was water-limited in 2019 (causal effect of SWC and WTD were higher relative to energy-related factors) (Figure 11a). The sudden shift from energy to water limitation of GPP is caused by surface water drawback (SWC below ~82.5% field capacity and WTD below −8cm) (Figure 9b). In 2020, GPP was again driven by VPD and other energy-related factors. This is because SWC did not drop below 82.5% in 2019.

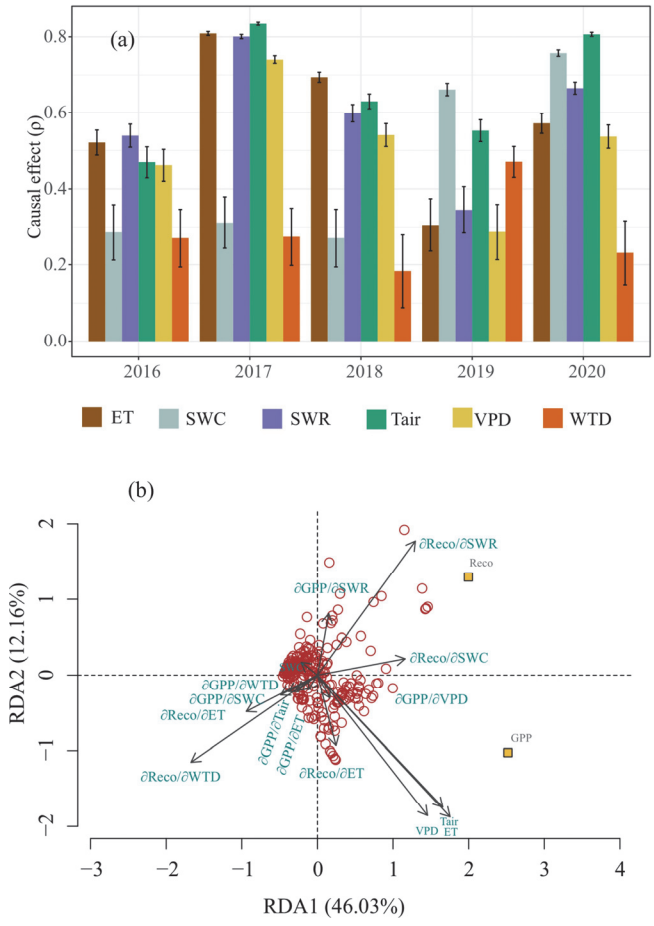

Figure 11: Causal inference of the impact of energy and water limitation on GPP. **a**: Cross-map skill at convergence retrieved using the CCM analysis. Each of the bars represents the effect of the predictors on GPP (ET:GPP, VPD:GPP, etc) for each year. Missing bars represent non-significant ($\rho = 0$) effects. **b**: RDA analysis showing the impact of causal interactions on GPP and Reco at a weekly time step (Source: Article IV).

Causal directions of GPP (δGPP) and Reco ($\delta Reco$) were explored combining s-maps, and RDA (Figure 11b). The magnitude was then further asserted by the variable importance graph (Figure 12). Causal strength of Tair on Reco ($\delta Reco/\delta Tair$), SWC on Reco ($\delta Reco/\delta SWC$), and VPD on GPP ($\delta GPP/\delta VPD$) were positively impacting GPP. Nevertheless, causal impacts of SWC on GPP ($\delta GPP/\delta SWC$), WTD on GPP ($\delta GPP/\delta WTD$), SWR on GPP ($\delta GPP/\delta SWR$), ET on Reco ($\delta Reco/\delta ET$) had negative effects on GPP (i.e. Burns Bog preferred water retention over C assimilation). Meanwhile, causal strength of ET on GPP ($\delta GPP/\delta ET$), Tair on GPP ($\delta GPP/\delta Tair$), and Reco on WTD ($\delta Reco/\delta WTD$) had positive correlations with GPP.

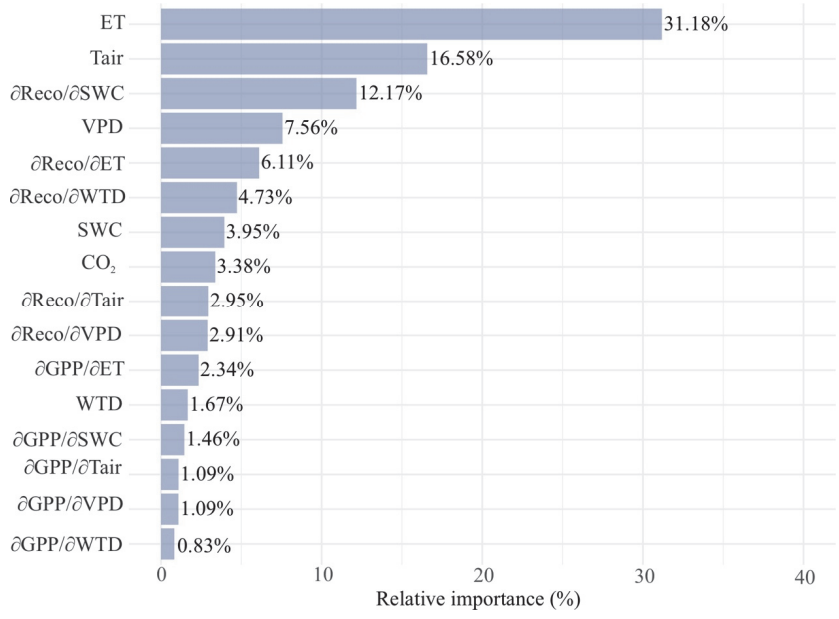

Figure 12: Relative variable importance of causal interactions, carbon and energy- related parameters on GPP. The relative variable importance was extracted from random forest regression with 500 trees, with the model expanding 66% of the variance in GPP with a root-mean-square error of 0.55 g C m^{-2} day^{-1} (Source: Article IV).

3.2. CO_2 fertilisation effect on C balance (Article III)

3.2.1. Ecosystem scale C balance

Analysis with CARDAMOM calibrated DALEC estimates revealed that Bonanza Creek rich fen peatland was a slight sink of CO_2 across the seven-year study period. The simplistic representation of the C dynamics at the site below attests this analysis (Figure 13). The annual estimates are generated from the weekly time step probabilistic CARDAMOM outputs. The fen peatland on average fixed 543.9 g C m^{-2} $year^{-1}$. After respiring 257.5 g C m^{-2} y^{-1} back to the atmosphere as R_a, the ecosystem allocated NPP of 286.5 g C m^{-2} y^{-1} to the four live biomass pools. CUE of Bonanza Creek was 0.52. On average 129.8 g C m^{-2} y^{-1} of NPP was allocated to foliage C pool. But the fine root and structural C pools received only 56.1 g C m^{-2} y^{-1} and 88.8 g C m^{-2} y^{-1} respectively. The analysis implied that labile C pool takes up the second largest share of the NPP after foliage (116.9 g C m^{-2} y^{-1}) which was used for leaf flushing during the ensuing spring onset.

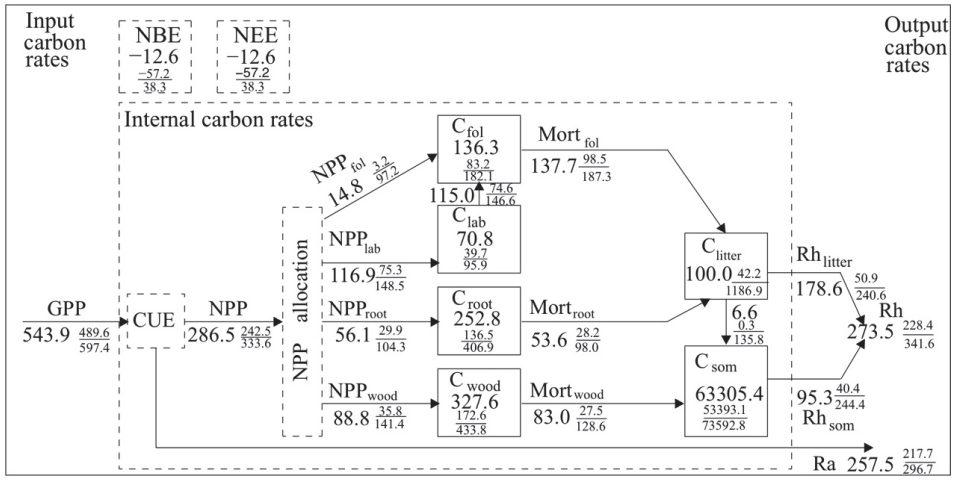

Figure 13: CARDAMOM C-cycle analysis of Bonanza Creek rich fen peatland (Alaska). Numbers show a median estimate of fluxes (alongside arrows) and of stocks (in boxes). Units are g C m^{-2} for stocks and g C m^{-2} y^{-1} for fluxes. 95% CI is shown in a fractional form with 2.5 and 97.5 percentiles as numerator and denominator. Black fluxes are biogenic, including NPP, mortality (Mort), R_a, and R_h. NEE = R_a + R_h – GPP. Net biome exchange = NEE – disturbance fluxes. Since there were no fire events, net biome exchange is the same as NEE. Wood in the subscripts indicates structural C (coarse roots, stems, and branches where applicable) of the plants. (Source: Article III)

CARDAMOM profiled estimates were validated with the data which were not part of the assimilation. The SOC stock, BG and AG NPP and FRC stock were validated with independent in-situ measurements. DALEC estimate of the FRC stock; 252.8 g C m^{-2} (Figure 13 & Figure 16) It accurately represented the site biophysical conditions (in-situ data 247 g C m^{-2}, (McConnell et al., 2013; A meta-analysis of published literature is provided in the supplementary file of Article III). CARDAMOM profiled mean annual estimates of structural, labile and foliage C stock are shown in Figures 13 & 16b). The analysis additionally revealed the average litter C pool (Figure 16b). Finally, 6.6 and 83 g C m^{-2} y^{-1} of the litter and structural C pools, respectively, was decomposed. The decomposition contributed to an R_h of 273.5 g C m^{-2} y^{-1} (Figure 14).

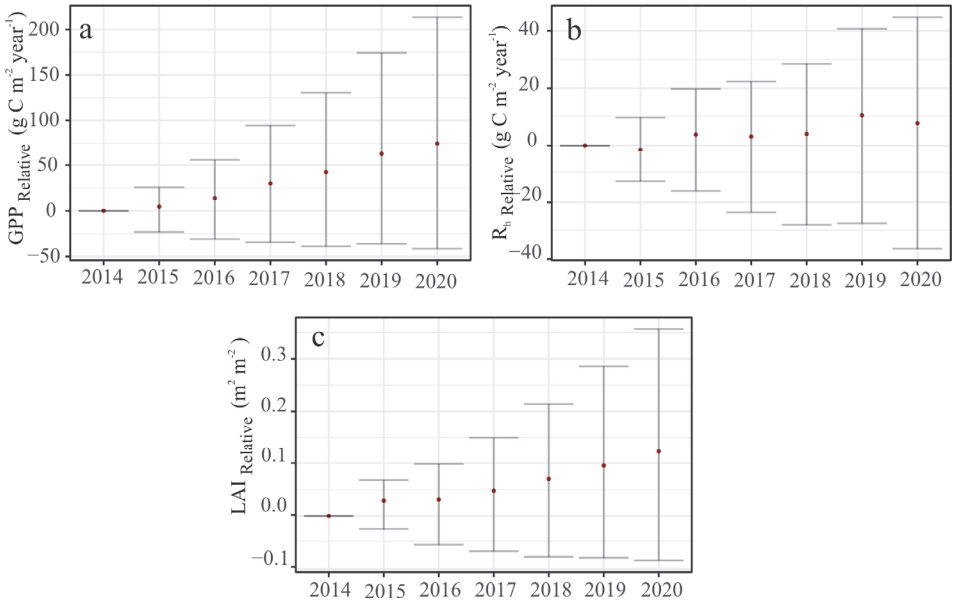

Figure 14: CO_2 balance of Bonanza Creek explained by relative change in C variables. **a**: GPP, **b**: R_h, and **c**: LAI. The points indicate the relative change in a median estimate with respect to 2014. The error bars represent relative change in the 95% CI from the year 2014. These are estimated based on the CARDAMOM calibrated DALEC weekly time step outputs. (Source: Article III)

The increasing net C sink strength was driven by a positive GPP (Figure 14a) and R_h was relatively constant (Figure 14b). A positive greening trend, as suggested by LAI, corroborates the increasing GPP. GPP increased by ~75 g C m^{-2} y^{-1} by 2020. R_h, increasing only by ~8 g C m^{-2} $year^{-1}$ did not significantly reduce the ecosystem sink strength.

3.2.2. Model diagnostic analysis

The synthetic experiments with the calibrated DALEC model and the ACM-1 photosynthetic sub-model showed a CO_2 fertilisation effect driving GPP. An initial correlation analysis with atmospheric CO_2 concentration explained ~29% variation in GPP (R^2 = 0.29, p value = 0.13, residual standard error = 23.53 at 5 degrees of freedom). LAI, on the other hand, had a strong correlation with GPP (R^2 = 0.96, p-value = <0.05, RSE = 5.35 with 5 degrees of freedom). This study also reports the synergistic and individual contributions of increasing atmospheric CO_2 concentration and LAI on GPP. Using the fixed CO_2 and climate experiment it was evident CO_2 fertilisation caused the positive GPP and LAI trend (Figure 15c & d). Finally, using the ACM-1 sub-model experiment, it was found that the direct contribution of CO_2 effect on GPP growth was ~14%. The indirect effect of CO_2 fertilisation on GPP positive trend through increased LAI was ~4%. DALEC revealed similar effects in the NEE and Reco estimates. The

fixed climate experiment did not show any independent climate–carbon feedback, suggesting that the effect is restricted to CO_2 fertilisation. Furthermore, we did not see any changes in GPP compared to CARDAMOM estimates, when the sub-model ACM-1 was driven by the same synthetic meteorological datasets used in the fixed CO_2 and climate experiments and thus separated the indirect CO_2 fertilisation effect through changes in LAI.

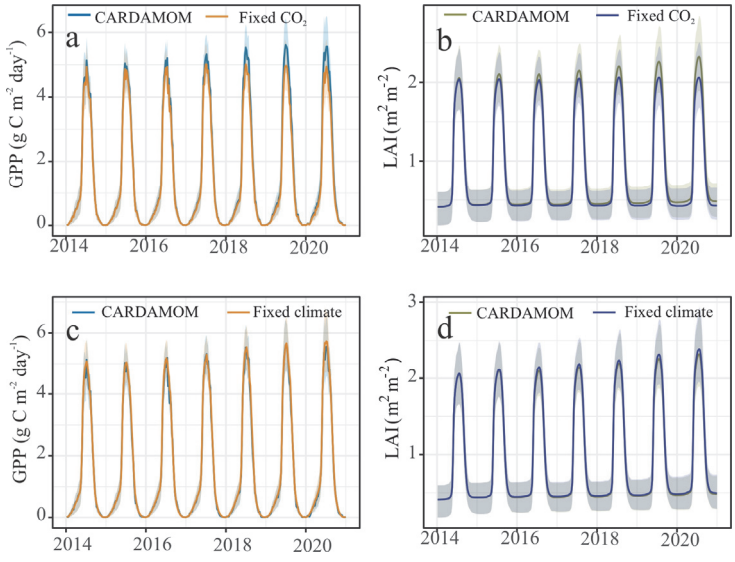

Figure 15: The greening and the subsequent increase in the production is forced by CO_2 fertilisation effect. **a**: The positive inter-annual trend seen in GPP is explained by the comparison between CARDAMOM profiled estimates and the DALEC diagnostic synthetic experiments (a): Fixed CO_2 outcome for GPP, and **b**: LAI. Fixed climatic synthetic experiment outcome for **c**: GPP and **d**: LAI. The shaded regions represent the respective 95% CI.

3.3.3. Photosynthate allocation and C residence times

The rich fen favoured foliage (50% of NPP) over fine root (20% of NPP) and structural (woody C pool) C pool (30% of NPP) photosynthate allocation (Figure 16). The fine roots and woody C pools are estimated to have a C residence time of 4.6 years. This is supported by published literature (see the supplementary file of Article III).

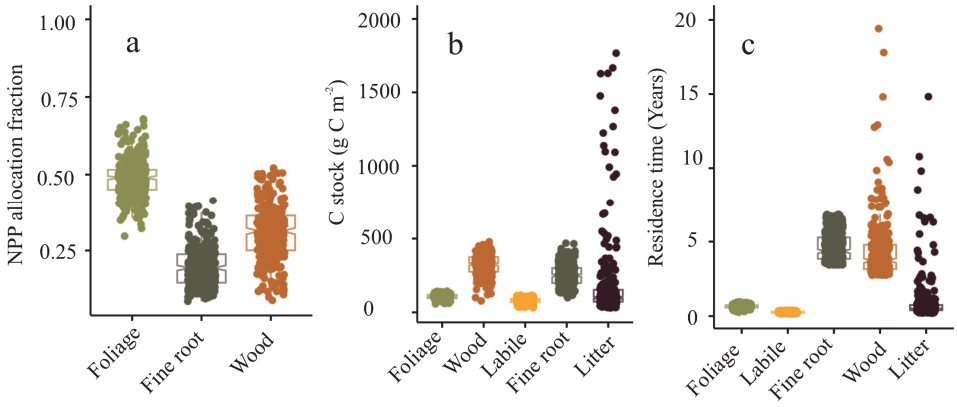

Figure 16: Internal C traits of Bonanza Creek rich fen ecosystem. **a**: Mean annual NPP allocation fractions **b**: Average C stock of foliage, woody, labile, fine root, and litter C pools and **c**: atmospheric CO_2 concentration. Comparison between the weekly posterior probability estimates of **c**: C residence times of foliage, labile, fine root, woody, and litter C pools. These metrics are estimated from the 300 ensemble members. The points indicate respective ensemble members (Source: Article III).

4. DISCUSSION

Peatlands, with their unique C-rich soils, are an essential component of the global land C budget. Understanding ecosystem resilience to the projected anthropogenic and climatic impacts on land–atmosphere GHG exchange, especially CO_2 is unequivocally important for reducing the uncertainties associated with the global C budget. Predicting future responses of peatlands and their biogeochemical cycles necessitates improving the past and present movement of CO_2 and other GHG fluxes and related microtechnological parameters in the soil–plant–atmosphere continuum. This thesis addressed the above knowledge-gaps through four research articles covered here.

4.1. Synthesis: Soil moisture and GHG exchange (Articles I, II, III & IV)

Water transport through the soil–plant–atmosphere continuum critically impacts GPP (Green et al., 2019; Peng et al., 2024; Wang et al., 2022). However, accurately characterising the response of C and N fluxes to soil moisture in process-based models of C is challenging, leading to uncertainties in the quantification of climate–carbon feedbacks (Kannenberg et al., 2024). This uncertainty is caused primarily by the lack of process-based understanding of the relationship between soil moisture and GPP. The uncertainty further propagates to photosynthate allocation, mortality rates, residence times, and in the end to NEE. There are several debates against and for the role of soil moisture in GPP limitation especially under climate change and intensifying extreme climatic events (Kannenberg et al., 2024; Novick et al., 2016; Voigt et al., 2024; Wang et al., 2022; Zhang et al., 2016). I found a Gaussian response by both NEE and GHG across the varying soil moisture spectrum (Articles I and II). This finding contradicts the existing evidence of a positive linear response (Evans et al., 2021). Also see Quan et al., (2019), Taylor et al., (2017), and Wang et al., (2014). Inferences made from the analysis also clearly indicated CO_2 as the dominant GHG (Figure 3). This is supported by the conclusions drawn by several studies (IPCC, 2023; Evans et al., 2021; Huang et al., 2021) with notable exceptions (Covey et al., 2021; Minkkinen et al., 2002). While Evans et al., (2021) and Quan et al., (2019) covered with measurements spanning longer time periods (years), Articles I and II lacked the temporal dynamics. N_2O contributed 33% to GHG exchange in GHG source sites (i.e. drained floodplain meadows and cultivated fields). However, it only contributed ~10% in drained grassland sites.

I addressed the data and knowledge-gaps in article I and II by specifically focusing on single sites — ecosystem scale EC data from sub-Arctic (Article III) and temperate (Article IV) peatlands. Bonanza Creek (Article III) was flooded (60 cm above the peat surface) throughout the study period (2014 to 2020). Soil moisture did not have any role in variability seen in GPP and NEE across growing

season specific, and weekly time step data. This directly contradicts the findings from Article I and II and published literature (Evans et al., 2021; Peng et al., 2024; Quan et al., 2019). It led to the hypothesis that the soil moisture and photosynthesis relationship is coupled with one or more meteorological drivers not covered in Articles I, II and III. Furthermore, it can also be explained by a soil moisture minimum at which it starts to have an impact on photosynthesis. Article IV explicitly tested these hypotheses by investigating the hydro-climatic impacts on GPP in an atmospheric drought (high VPD) affected temperate restored bog peatland. Spatial and temporal dynamics of energy and water limitation of terrestrial GPP are central to understanding ecosystem CO_2 dynamics and related uncertainties in dry and drought-affected zones (Ahmad et al., 2024; Fu et al., 2022; Heijmans et al., 2004; Kim & Verma, 1996; Schwingshackl et al., 2017; Seneviratne et al., 2010). Peatlands may experience diverse dire climate–carbon feedbacks to temporal dynamics of energy and water limitation, as they are the largest reservoirs of C. This brings the dynamics of the VPD–SWC–GPP relationship in the soil–plant–atmosphere continuum into the forefront of C cycle ecology.

In the first three years of the study, GPP was not limited by soil moisture (Figure 10b, Table 4); instead, it was influenced by the presence or absence of physiological control exerted by vascular plants to mitigate drought stress. Drought stress was driven by changes in Tair and VPD, a finding strongly supported in the literature (Grossiord et al., 2020; Novick et al., 2016). The isohydric phenomena led to the plant–water stress, contradicting the findings of canopy regulation in non-forested ecosystems to droughts (Zhang et al., 2016). This means that peatlands prefer to minimize water loss over C assimilation (line II Figure 2,). This might be why GPP was around 2.5 g C m^{-2} day^{-1} during the drought severe periods (Figure 9. i.e. a decline in GPP is experienced as hypothesised in line II, Figure 2). However, the non-forested ecosystems were grasslands and open shrublands (Zhang et al., 2016). Access to copious amounts of water and sphagnum dominance in comparison to shrublands or grasslands could be why the bog mimicked the forest ecosystem responses to drought as seen in Zhang et al., (2016). Findings of this study also differ from the diminished VPD suppression of vegetation growth in northern peatlands (Chen et al., 2023). The reduction in the VPD suppression of GPP may be influenced by soil moisture variability seen in this study. As the climate warms and droughts get more severe, the dual nature of GPP limitation, as seen here, could become more evident in the future. The decline in the severity of drought in the following years (2017 and 2018) could have resulted in a relaxed physiological regulation to maximise C assimilation by the vascular plants (Chen et al., 2023).

Overall, my findings lead to hypothesise existence of regional and/or biome specific soil moisture relationship with GPP and NEE. This dynamic relationship can be further amplified or diminished due to extreme climatic events caused by climate–carbon feedbacks (Article IV) and climate change (Article III).

4.2. Innovations, novelties, limitations, and future steps in C and N cycle research

Article I and II provided the basic empirical knowledge required to advance on the role of soil moisture on GHG exchange. It further pointed out microbiome as second most factor to explain GHG and more specifically C spatial variability. The dominant role of CO_2 fluxes in GHG exchange as seen in Articles I and II lead to Article III focusing on C cycle. Further introspection with model–data fusion approach, and subsequent diagnostic analysis, Article III provided a benchmark representation of average C balance, synergistic and indirect effect of CO_2 fertilisation effect at ecosystem scale. Although, a manipulation experiment in a sedge-dominated boreal peatland showed the effect of temperature and atmospheric CO_2 on GPP (Tian et al., 2020), article could be the first long-term ecosystem-scale study to partition between effects on peatland C dynamics. However, temperature (McPartland et al., 2019), precipitation and SWR did not have any effect on GPP in Bonanza Creek. Also, there is recent evidence on both individual and synergistic effects of climatic factors on plant community structure, species abundance, and succession.

There is also a growing consensus on the nutrient (e.g. N limitation) and soil moisture limitation of CO_2 fertilisation effect. Soil moisture limitation was not observed because Bonanza Creek was flooded (Article III). CO_2 fertilisation effect was also not evident in Burns Bog (Article IV). There are several evidence on N limitation of biomass synthesis (foliar nitrogen is a crucial component of photosynthesis). This is because of the limited supply of plant available N (NO_3^- and NH_4^+) in the soil for the observed positive greening trend (CO_2 fertilisation effect). Microbial demand for NO_3^- and NH_4^+ can also complicate photosynthesis. These processes can have divergent effects on global C cycle and could even reduce current uncertainties in IAV of land C cycle (Friedlingstein et al., 2025; Stocker et al., 2025). This could probably one of the reasons why the uncertainty dominated the mean estimates. This underscores the requirement of including N limitation and C–N coupling processes in terrestrial C cycle models.

Finally, Article III provided insights into ecosystem scale internal C traits (C residence times and photosynthate allocation) with uncertainty characterisation (data assimilation). To the best of my knowledge, this is the first study to provide peatland specific plant tissue allocation fractional rates and C residence times of C biomass pools. More specifically, the greening trend seen in the findings also meant the foliage allocation is favoured over fine root and structural C pools. This could be due to the climate warming and CO_2 fertilisation effect at the site scale. This goes against the consensus that these effects force the plants to allocate more C to fine roots (Malhotra et al., 2020). However, since the fen peatland was flooded for most of the study period, it was not necessary to retrieve water from the deeper soil horizon. Thus, the longer fine roots were not present. This could explain the relatively lower photosynthate allocation to fine roots (Weltzin et al., 2000). Similar fine root allocation patterns have been reported from the northern bog and fen ecosystems (Mäkiranta et al., 2018; Murphy & Moore, 2010).

5. CONCLUSION

Climate warming and extreme climatic events are expected to intensify before the turn of the century exposing peat soils. Findings outlined in this thesis indicate ecosystem scale differences in spatio-temporal variations in hydro-climatic impact on GHG, specifically, GPP. The unimodal relationship of GHG and NEE across a soil moisture spectrum (0.2 m^3 m^{-3} to 1 m^3 m^{-3}) defy findings reported by Articles III and IV. Although the data covered in the study (Article I) have spatial coverage (48 sites), it is weak on the temporal resolution (3–4 days at each site). Article II specifically focused on tropical peatlands. While CO_2 dominated GHG exchange in net absorption sites, N_2O was the dominant in GHG source sites. On the other hand, CARDAMOM calibrated DALEC at weekly time step for seven years found CO_2 effect on GPP in a sub-Arctic site (Article III). Soil moisture did not have any impact on GPP. Bonanza Creek was flooded for most part of the study period. This might be why soil moisture did not have any role in GPP. This study was the first (to the best of my knowledge) ecosystem-scale analysis to provide C allocation rates and residence times of various C pools. Furthermore, this study also provided the individual and synergistic impact of CO_2 fertilisation on GPP. I also provided exhaustive and comprehensive uncertainty characterisation for the parameters, fluxes, and C stocks. On the contrary, the fourth study (Article IV) found a negative effect of soil moisture effect on GPP in a drought-affected restored bog. The analysis found a soil moisture threshold of 82.5%, below which water scarcity starts to limit GPP. VPD was the limiting factor for GPP unless it had not been restricted by plant water stress. Plant hydraulic responses to atmospheric drought were the underlying cause for the soil moisture drawback.

REFERENCES

Admiral, S. W., & Lafleur, P. M. (2007). Partitioning of latent heat flux at a northern peatland. *Aquatic Botany*, 86(2), 107-116. https://doi.org/10.1016/j.aquabot.2006.09.006

Ahmad, S. K., Holmes, T. R., Kumar, S. V., Lahmers, T. M., Liu, P.-W., Nie, W., Getirana, A., Orland, E., Bindlish, R., Guzman, A., Hain, C. R., Melton, F. S., Locke, K. A., & Yang, Y. (2024). Droughts impede water balance recovery from fires in the Western United States. *Nature Ecology & Evolution*, 8(2), 229–238. https://doi.org/10.1038/s41559-023-02266-8

Antala, M., Juszczak, R., van der Tol, C., & Rastogi, A. (2022). Impact of climate change-induced alterations in peatland vegetation phenology and composition on carbon balance. *Science of The Total Environment*, 827, 154294. https://doi.org/10.1016/j.scitotenv.2022.154294

Bahram, M., Espenberg, M., Pärn, J., Lehtovirta-Morley, L., Anslan, S., Kasak, K., Kõljalg, U., Liira, J., Maddison, M., Moora, M., Niinemets, Ü., Öpik, M., Pärtel, M., Soosaar, K., Zobel, M., Hildebrand, F., Tedersoo, L., & Mander, Ü. (2022). Structure and function of the soil microbiome underlying N_2O emissions from global wetlands. *Nature Communications*, *13*(1), 1430. https://doi.org/10.1038/s41467-022-29161-3

Bardgett, R. D., Streeter, T. C., & Bol, R. (2003). Soil microbes compete effectively with plants for organic-nitrogen inputs to temperate grasslands. *Ecology*, 84(5), 1277–1287. https://doi.org/10.1890/0012-9658(2003)084[1277:SMCEWP]2.0.CO;2

Bassiouni, M., Good, S. P., Still, C. J., & Higgins, C. W. (2020). Plant water uptake thresholds inferred from satellite soil moisture. *Geophysical Research Letters*, 47(7), e2020GL087077. https://doi.org/10.1029/2020GL087077

Batjes, N. H. (2014). Total carbon and nitrogen in the soils of the world. *European Journal of Soil Science*, *65*(1), 10–21. https://doi.org/10.1111/ejss.12114_2

Beguería, S., Vicente-Serrano, S. M., Reig, F., & Latorre, B. (2014). Standardized precipitation evapotranspiration index (SPEI) revisited: Parameter fitting, evapotranspiration models, tools, datasets and drought monitoring. *International Journal of Climatology*, *34*(10), 3001–3023. https://doi.org/10.1002/joc.3887

Berner, L. T., Massey, R., Jantz, P., Forbes, B. C., Macias-Fauria, M., Myers-Smith, I., Kumpula, T., Gauthier, G., Andreu-Hayles, L., Gaglioti, B. V., Burns, P., Zetterberg, P., D'Arrigo, R., & Goetz, S. J. (2020). Summer warming explains widespread but not uniform greening in the Arctic tundra biome. *Nature Communications*, *11*(1), Article 1. https://doi.org/10.1038/s41467-020-18479-5

Bloom, A. A., Exbrayat, J.-F., van der Velde, I. R., Feng, L., & Williams, M. (2016). The decadal state of the terrestrial carbon cycle: Global retrievals of terrestrial carbon allocation, pools, and residence times. *Proceedings of the National Academy of Sciences*, *113*(5), 1285–1290. https://doi.org/10.1073/pnas.1515160113

Bloom, A. A., Palmer, P. I., Fraser, A., Reay, D. S., & Frankenberg, C. (2010). Large-scale controls of methanogenesis inferred from methane and gravity spaceborne data. *Science*, *327*(5963), 322–325. https://doi.org/10.1126/science.1175176

Bloom, A. A., & Williams, M. (2015). Constraining ecosystem carbon dynamics in a data-limited world: Integrating ecological "common sense" in a model–data fusion framework. *Biogeosciences*, *12*(5), 1299–1315. https://doi.org/10.5194/bg-12-1299-2015

Breshears, D. D., Adams, H. D., Eamus, D., McDowell, N., Law, D. J., Will, R. E., Williams, A. P., & Zou, C. B. (2013). The critical amplifying role of increasing atmospheric moisture demand on tree mortality and associated regional die-off. *Frontiers in Plant Science*, *4*. https://doi.org/10.3389/fpls.2013.00266

Chaudhary, N., Westermann, S., Lamba, S., Shurpali, N., Sannel, A. B. K., Schurgers, G., Miller, P. A., & Smith, B. (2020). Modelling past and future peatland carbon dynamics across the pan-Arctic. *Global Change Biology*, *26*(7), 4119–4133. https://doi.org/10.1111/gcb.15099

Chen, N., Zhang, Y., Yuan, F., Song, C., Xu, M., Wang, Q., Hao, G., Bao, T., Zuo, Y., Liu, J., Zhang, T., Song, Y., Sun, L., Guo, Y., Zhang, H., Ma, G., Du, Y., Xu, X., & Wang, X. (2023). Warming-induced vapor pressure deficit suppression of vegetation growth diminished in northern peatlands. *Nature Communications*, *14*(1), 7885. https://doi.org/10.1038/s41467-023-42932-w

Christen, A., & Knox, S. (2022). *AmeriFlux FLUXNET-1F CA-DBB Delta Burns Bog* [Dataset]. AmeriFlux; University of British Columbia. https://doi.org/10.17190/AMF/1881565

Churchill, A. C., Turetsky, M. R., McGuire, A. D., & Hollingsworth, T. N. (2015). Response of plant community structure and primary productivity to experimental drought and flooding in an Alaskan fen. *Canadian Journal of Forest Research*, *45*(2), 185–193. https://doi.org/10.1139/cjfr-2014-0100

Collalti, A., Ibrom, A., Stockmarr, A., Cescatti, A., Alkama, R., Fernández-Martínez, M., Matteucci, G., Sitch, S., Friedlingstein, P., Ciais, P., Goll, D. S., Nabel, J. E. M. S., Pongratz, J., Arneth, A., Haverd, V., & Prentice, I. C. (2020). Forest production efficiency increases with growth temperature. *Nature Communications*, *11*(1), 5322. https://doi.org/10.1038/s41467-020-19187-w

Covey, K., Soper, F., Pangala, S., Bernardino, A., Pagliaro, Z., Basso, L., ... & Elmore, A. (2021). Carbon and beyond: The biogeochemistry of climate in a rapidly changing Amazon. *Frontiers in Forests and Global Change*, 4, 618401. https://doi.org/10.3389/ffgc.2021.618401

Davidson, S. J., Goud, E. M., Malhotra, A., Estey, C. O., Korsah, P., & Strack, M. (2021). Linear disturbances shift boreal peatland plant communities toward earlier peak greenness. *Journal of Geophysical Research: Biogeosciences*, *126*(8). https://doi.org/10.1029/2021JG006403

De Deyn, G. B., Cornelissen, J. H. C., & Bardgett, R. D. (2008). Plant functional traits and soil carbon sequestration in contrasting biomes. *Ecology Letters*, *11*(5), 516–531. https://doi.org/10.1111/j.1461-0248.2008.01164.x

DeColibus, D. T., Rober, A. R., Sampson, A. M., Shurzinske, A. C., Walls, J. T., Turetsky, M. R., & Wyatt, K. H. (2017). Legacy effects of drought alters the aquatic food web of a northern boreal peatland. *Freshwater Biology*, *62*(8), 1377–1388. https://doi.org/10.1111/fwb.12950

Deyle, E. R., May, R. M., Munch, S. B., & Sugihara, G. (2016). Tracking and forecasting ecosystem interactions in real time. *Proceedings of the Royal Society B: Biological Sciences*, *283*(1822), 20152258. https://doi.org/10.1098/rspb.2015.2258

Deyle, E. R., & Sugihara, G. (2011). Generalized theorems for nonlinear state space reconstruction. *Plos One*, *6*(3), e18295. https://doi.org/10.1371/journal.pone.0018295

Dorrepaal, E., Aerts, R., Cornelissen, J. H. C., Callaghan, T. V., & Van Logtestijn, R. S. P. (2004). Summer warming and increased winter snow cover affect *Sphagnum fuscum* growth, structure and production in a sub-Arctic bog. *Global Change Biology*, *10*(1), 93–104. https://doi.org/10.1111/j.1365-2486.2003.00718.x

Euskirchen, E. S. (2022a). *AmeriFlux FLUXNET-1F US-BZF Bonanza Creek Rich Fen* [Dataset]. AmeriFlux; University of Alaska Fairbanks, Institute of Arctic Biology. https://doi.org/10.17190/AMF/1881570

Euskirchen, E. S. (2022b). *AmeriFlux FLUXNET-1F US-BZS Bonanza Creek Black Spruce* [Dataset]. AmeriFlux; University of Alaska Fairbanks, Institute of Arctic Biology. https://doi.org/10.17190/AMF/1881572

Euskirchen, E. S., Kane, E. S., Edgar, C. W., & Turetsky, M. R. (2020). When the source of flooding matters: Divergent responses in carbon fluxes in an Alaskan rich fen to two types of inundation. *Ecosystems*, *23*(6), 1138–1153. https://doi.org/10.1007/s10021-019-00460-z

Evans, C. D., Peacock, M., Baird, A. J., Artz, R. R. E., Burden, A., Callaghan, N., ... & Morrison, R. (2021). Overriding water table control on managed peatland greenhouse gas emissions. *Nature*, *593*(7860), 548-552. https://doi.org/10.1038/s41586-021-03523-1

Famiglietti, C. A., Smallman, T. L., Levine, P. A., Flack-Prain, S., Quetin, G. R., Meyer, V., Parazoo, N. C., Stettz, S. G., Yang, Y., Bonal, D., Bloom, A. A., Williams, M., & Konings, A. G. (2021). Optimal model complexity for terrestrial carbon cycle prediction. *Biogeosciences*, *18*(8), 2727–2754. https://doi.org/10.5194/bg-18-2727-2021

Fan, Z., David McGuire, A., Turetsky, M. R., Harden, J. W., Michael Waddington, J., & Kane, E. S. (2013). The response of soil organic carbon of a rich fen peatland in interior Alaska to projected climate change. *Global Change Biology*, *19*(2), 604–620. https://doi.org/10.1111/gcb.12041

FAO. (2011*). Classification of organic soils*. Food and Agriculture Organization of the United Nations.

Fenner, N., & Freeman, C. (2011). Drought-induced carbon loss in peatlands. *Nature Geoscience*, *4*(12), 895–900. https://doi.org/10.1038/ngeo1323

Freeman, B. W. J., Evans, C. D., Musarika, S., Morrison, R., Newman, T. R., Page, S. E., Wiggs, G. F. S., Bell, N. G. A., Styles, D., Wen, Y., Chadwick, D. R., & Jones, D. L. (2022). Responsible agriculture must adapt to the wetland character of mid-latitude peatlands. *Global Change Biology*, *28*(12), 3795–3811. https://doi.org/10.1111/gcb.16152

Friedlingstein, P., O'Sullivan, M., Jones, M. W., Andrew, R. M., Hauck, J., Landschützer, P., Le Quéré, C., …& Zeng, J. (2025). Global carbon budget 2024. *Earth System Science Data*, *17*(3), 965–1039. https://doi.org/10.5194/essd-17-965-2025

Frolking, S., Talbot, J., Jones, M. C., Treat, C. C., Kauffman, J. B., Tuittila, E.-S., & Roulet, N. (2011). Peatlands in the Earth's 21st century climate system. *Environmental Reviews*, *19*, 371–396. https://doi.org/10.1139/a11-014

Fu, Z., Ciais, P., Prentice, I. C., Gentine, P., Makowski, D., Bastos, A., Luo, X., Green, J. K., Stoy, P. C., Yang, H., & Hajima, T. (2022). Atmospheric dryness reduces photosynthesis along a large range of soil water deficits. *Nature Communications*, *13*(1), 989. https://doi.org/10.1038/s41467-022-28652-7

Fuster, B., Sánchez-Zapero, J., Camacho, F., García-Santos, V., Verger, A., Lacaze, R., ... & Smets, B. (2020). Quality assessment of PROBA-V LAI, fAPAR and fCOVER collection 300 m products of Copernicus global land service. *Remote Sensing*, *12*(6), 1017. https://doi.org/10.3390/rs12061017

Gentine, P., Green, J. K., Guérin, M., Humphrey, V., Seneviratne, S. I., Zhang, Y., & Zhou, S. (2019). Coupling between the terrestrial carbon and water cycles—A review. *Environmental Research Letters*, *14*(8), 083003. https://doi.org/10.1088/1748-9326/ab22d6

Gnambs, T. (2023). A brief note on the standard error of the Pearson correlation. *Collabra: Psychology*, *9*(1), 87615. https://doi.org/10.1525/collabra.87615

Gougoulias, C., Clark, J. M., & Shaw, L. J. (2014). The role of soil microbes in the global carbon cycle: Tracking the below-ground microbial processing of plant-derived carbon for manipulating carbon dynamics in agricultural systems. *Journal of the Science of Food and Agriculture*, *94*(12), 2362–2371. https://doi.org/10.1002/jsfa.6577

Green, J. K., Seneviratne, S. I., Berg, A. M., Findell, K. L., Hagemann, S., Lawrence, D. M., & Gentine, P. (2019). Large influence of soil moisture on long-term terrestrial carbon uptake. *Nature*, *565*(7740), 476–479. https://doi.org/10.1038/s41586-018-0848-x

Grossiord, C., Buckley, T. N., Cernusak, L. A., Novick, K. A., Poulter, B., Siegwolf, R. T. W., Sperry, J. S., & McDowell, N. G. (2020). Plant responses to rising vapor pressure deficit. *New Phytologist*, *226*(6), 1550–1566. https://doi.org/10.1111/nph.16485

Guay, K. C., Beck, P. S. A., Berner, L. T., Goetz, S. J., Baccini, A., & Buermann, W. (2014). Vegetation productivity patterns at high northern latitudes: A multi-sensor satellite data assessment. *Global Change Biology*, *20*(10), 3147–3158. https://doi.org/10.1111/gcb.12647

Günther, A., Barthelmes, A., Huth, V., Joosten, H., Jurasinski, G., Koebsch, F., & Couwenberg, J. (2020). Prompt rewetting of drained peatlands reduces climate warming despite methane emissions. *Nature Communications*, *11*(1), 1644. https://doi.org/10.1038/s41467-020-15499-z

Haario, H., Saksman, E., & Tamminen, J. (2001). An adaptive metropolis algorithm. *Bernoulli*, *7*(2), 223–242. https://doi.org/10.2307/3318737

Heijmans, M. P. D., Arp, W. J., & Chapin III, F. S. (2004). Controls on moss evaporation in a boreal black spruce forest. *Global Biogeochemical Cycles*, *18*(2). https://doi.org/10.1029/2003GB002128

Hermle, S., Lavigne, M. B., Bernier, P. Y., Bergeron, O., & Paré, D. (2010). Component respiration, ecosystem respiration and net primary production of a mature black spruce forest in northern Quebec. *Tree Physiology*, *30*(4), 527–540. https://doi.org/10.1093/treephys/tpq002

Hill, T. C., Ryan, E., & Williams, M. (2012). The use of CO_2 flux time series for parameter and carbon stock estimation in carbon cycle research. *Global Change Biology*, *18*(1), 179–193. https://doi.org/10.1111/j.1365-2486.2011.02511.x

Huang, Y., Ciais, P., Luo, Y., Zhu, D., Wang, Y., Qiu, C., ... & Qu, L. (2021). Tradeoff of CO_2 and CH_4 emissions from global peatlands under water-table drawdown. *Nature Climate Change*, *11*(7), 618–622. https://doi.org/10.1038/s41558-021-01059-w

IPCC. (2023). Summary for policymakers. In: Climate Change 2023: Synthesis report. contribution of working groups I, II and III to the Sixth Assessment Report of the Intergovernmental Panel on Climate Change [Core writing team, H. Lee and J. Romero (eds.)]. *IPCC, Geneva, Switzerland*. 1–34. https://doi.org/10.59327/IPCC/AR6-9789291691647.001

Jauhiainen, J., Takahashi, H., Heikkinen, J. E. P., Martikainen, P. J., & Vasander, H. (2005). Carbon fluxes from a tropical peat swamp forest floor. *Global Change Biology*, *11*(10), 1788–1797. https://doi.org/10.1111/j.1365-2486.2005.001031.x

Ju, J., & Masek, J. G. (2016). The vegetation greenness trend in Canada and US Alaska from 1984–2012 Landsat data. *Remote Sensing of Environment*, *176*, 1–16. https://doi.org/10.1016/j.rse.2016.01.001

Kane, E. S., Dieleman, C. M., Rupp, D., Wyatt, K. H., Rober, A. R., & Turetsky, M. R. (2021). Consequences of increased variation in peatland hydrology for carbon storage: Legacy effects of drought and flood in a boreal fen ecosystem. *Frontiers in Earth Science*, *8*, 577746. https://doi.org/10.3389/feart.2020.577746

Kannenberg, S. A., Anderegg, W. R. L., Barnes, M. L., Dannenberg, M. P., & Knapp, A. K. (2024). Dominant role of soil moisture in mediating carbon and water fluxes in dryland ecosystems. *Nature Geoscience*, *17*(1), 38–43. https://doi.org/10.1038/s41561-023-01351-8

Kattge, J., Díaz, S., Lavorel, S., Prentice, I. C., Leadley, P., Bönisch, G., … & Wirth, C. (2011). TRY – a global database of plant traits. *Global Change Biology*, *17*(9), 2905–2935. https://doi.org/10.1111/j.1365-2486.2011.02451.x

Kaye, J. P., & Hart, S. C. (1997). Competition for nitrogen between plants and soil microorganisms. *Trends in Ecology & Evolution*, *12*(4), 139–143. https://doi.org/10.1016/S0169-5347(97)01001-X

Kettridge, N., & Waddington, J. M. (2014). Towards quantifying the negative feedback regulation of peatland evaporation to drought. *Hydrological Processes*, *28*(11), 3728–3740. https://doi.org/10.1002/hyp.9898

Kim, J., & Verma, S. B. (1996). Surface exchange of water vapour between an open sphagnum fen and the atmosphere. *Boundary-Layer Meteorology*, *79*(3), 243–264. https://doi.org/10.1007/BF00119440

Kleinen, T., Brovkin, V., & Schuldt, R. J. (2012). A dynamic model of wetland extent and peat accumulation: Results for the Holocene. *Biogeosciences*, *9*(1), 235–248. https://doi.org/10.5194/bg-9-235–2012

Knauer, J., El-Madany, T. S., Zaehle, S., & Migliavacca, M. (2018). Bigleaf–An R package for the calculation of physical and physiological ecosystem properties from eddy covariance data. *Plos One*, *13*(8), e0201114. https://doi.org/10.1371/journal.pone.0201114

Köster, E., Chapman, J. P. B., Barel, J. M., Korrensalo, A., Laine, A. M., Vasander, H. T., & Tuittila, E.-S. (2023). Water level drawdown makes boreal peatland vegetation more responsive to weather conditions. *Global Change Biology*, *29*(19), 5691–5705. https://doi.org/10.1111/gcb.16907

Kottek, M., Grieser, J., Beck, C., Rudolf, B., & Rubel, F. (2006). World map of the Köppen-Geiger climate classification updated. *Meteorologische Zeitschrift*, *15*(3), 259–263. https://doi.org/10.1127/0941-2948/2006/0130

Kugiumtzis, D. (1996). State space reconstruction parameters in the analysis of chaotic time series—The role of the time window length. *Physica D: Nonlinear Phenomena*, *95*(1), 13–28. https://doi.org/10.1016/0167-2789(96)00054-1

Kwon, M. J., Ballantyne, A., Ciais, P., Qiu, C., Salmon, E., Raoult, N., Guenet, B., Göckede, M., Euskirchen, E. S., Nykänen, H., Schuur, E. A. G., Turetsky, M. R., Dieleman, C. M., Kane, E. S., & Zona, D. (2022). Lowering water table reduces carbon sink strength and carbon stocks in northern peatlands. *Global Change Biology*, *28*(22), 6752–6770. https://doi.org/10.1111/gcb.16394

Laine, A. M., Mäkiranta, P., Laiho, R., Mehtätalo, L., Penttilä, T., Korrensalo, A., Minkkinen, K., Fritze, H., & Tuittila, E.-S. (2019). Warming impacts on boreal fen CO_2 exchange under wet and dry conditions. *Global Change Biology*, *25*(6), 1995–2008. https://doi.org/10.1111/gcb.14617

Lees, K. J., Quaife, T., Artz, R. R. E., Khomik, M., Sottocornola, M., Kiely, G., Hambley, G., Hill, T., Saunders, M., Cowie, N. R., Ritson, J., & Clark, J. M. (2019). A model of gross primary productivity based on satellite data suggests formerly afforested peatlands undergoing restoration regain full photosynthesis capacity after five to ten years. *Journal of Environmental Management*, *246*, 594–604. https://doi.org/10.1016/j.jenvman.2019.03.040

Leifeld, J., & Menichetti, L. (2018). The underappreciated potential of peatlands in global climate change mitigation strategies. *Nature Communications*, *9*(1), 1071. https://doi.org/10.1038/s41467-018-03406-6

Leifeld, J., Wüst-Galley, C., & Page, S. (2019). Intact and managed peatland soils as a source and sink of GHGs from 1850 to 2100. *Nature Climate Change*, *9*(12), 945–947. https://doi.org/10.1038/s41558-019-0615-5

Limpens, J., Berendse, F., Blodau, C., Canadell, J. G., Freeman, C., Holden, J., Roulet, N., Rydin, H., & Schaepman-Strub, G. (2008). Peatlands and the carbon cycle: From local processes to global implications – a synthesis. *Biogeosciences*, *5*(5), 1475–1491. https://doi.org/10.5194/bg-5-1475-2008

Loisel, J., Yu, Z., Beilman, D. W., Camill, P., Alm, J., Amesbury, M. J., … & Zhou, W. (2014). A database and synthesis of northern peatland soil properties and Holocene carbon and nitrogen accumulation. *The Holocene*, *24*(9), 1028–1042. https://doi.org/10.1177/0959683614538073

López, J., Way, D. A., & Sadok, W. (2021). Systemic effects of rising atmospheric vapor pressure deficit on plant physiology and productivity. *Global Change Biology*, *27*(9), 1704–1720. https://doi.org/10.1111/gcb.15548

Mäkiranta, P., Laiho, R., Mehtätalo, L., Straková, P., Sormunen, J., Minkkinen, K., Penttilä, T., Fritze, H., & Tuittila, E.-S (2018). Responses of phenology and biomass production of boreal fens to climate warming under different water-table level regimes. *Global Change Biology*, *24*(3), 944–956. https://doi.org/10.1111/gcb.13934

Malhotra, A., Brice, D. J., Childs, J., Graham, J. D., Hobbie, E. A., Vander Stel, H., Feron, S. C., Hanson, P. J., & Iversen, C. M. (2020). Peatland warming strongly increases fine-root growth. *Proceedings of the National Academy of Sciences*, *117*(30), 17627–17634. https://doi.org/10.1073/pnas.2003361117

Massman, W. J. (1999). A model study of kB_H^{-1} for vegetated surfaces using 'localized near-field' Lagrangian theory. *Journal of Hydrology*, *223*(1-2), 27–43. https://doi.org/10.1016/S0022-1694(99)00104-3

McConnell, N. A., Turetsky, M. R., McGuire, A. D., Kane, E. S., Waldrop, M. P., & Harden, J. W. (2013). Controls on ecosystem and root respiration across a permafrost and wetland gradient in interior Alaska. *Environmental Research Letters*, *8*(4), 045029. https://doi.org/10.1088/1748-9326/8/4/045029

McPartland, M. Y., Kane, E. S., Falkowski, M. J., Kolka, R., Turetsky, M. R., Palik, B., & Montgomery, R. A. (2019). The response of boreal peatland community composition and NDVI to hydrologic change, warming, and elevated carbon dioxide. *Global Change Biology*, *25*(1), 93–107. https://doi.org/10.1111/gcb.14465

Minkkinen, K., Korhonen, R., Savolainen, I., & Laine, J. (2002). Carbon balance and radiative forcing of Finnish peatlands 1900–2100 – the impact of forestry drainage. *Global Change Biology*, *8*(8), 785–799. https://doi.org/10.1046/j.1365-2486.2002.00504.x

Muller, F. L., Chang, K. C., Lee, C. L., & Chapman, S. J. (2015). Effects of temperature, rainfall and conifer felling practices on the surface water chemistry of northern peatlands. *Biogeochemistry*, *126*, 343–362. https://doi.org/10.1007/s10533-015-0162-8

Murdiyarso, D., Hergoualc'h, K., & Verchot, L. V. (2010). Opportunities for reducing greenhouse gas emissions in tropical peatlands. *Proceedings of the National Academy of Sciences*, *107*(46), 19655–19660. https://doi.org/10.1073/pnas.0911966107

Murphy, M. T., & Moore, T. R. (2010). Linking root production to aboveground plant characteristics and water table in a temperate bog. *Plant and Soil*, *336*(1), 219–231. https://doi.org/10.1007/s11104-010-0468-1

Myers-Smith, I. H., Kerby, J. T., Phoenix, G. K., Bjerke, J. W., Epstein, H. E., Assmann, J. J., ... & Wipf, S. (2020). Complexity revealed in the greening of the Arctic. *Nature Climate Change*, *10*(2), 106–117. https://doi.org/10.1038/s41558-019-0688-1

Nichols, D. S., & Brown, J. M. (1980). Evaporation from a sphagnum moss surface. *Journal of Hydrology*, *48*(3), 289–302. https://doi.org/10.1016/0022-1694(80)90121-3

Nichols, J. E., & Peteet, D. M. (2019). Rapid expansion of northern peatlands and doubled estimate of carbon storage. *Nature Geoscience*, *12*(11), 917–921. https://doi.org/10.1038/s41561-019-0454-z

Nisbet, E. G., Dlugokencky, E. J., & Bousquet, P. (2014). Methane on the rise—Again. *Science*, *343*(6170), 493–495. https://doi.org/10.1126/science.1247828

Niu, B., He, Y., Zhang, X., Zong, N., Fu, G., Shi, P., Zhang, Y., Du, M., & Zhang, J. (2017). Satellite-based inversion and field validation of autotrophic and heterotrophic respiration in an alpine meadow on the Tibetan Plateau. *Remote Sensing*, *9*(6), 615. https://doi.org/10.3390/rs9060615

Novick, K. A., Ficklin, D. L., Grossiord, C., Konings, A. G., Martínez-Vilalta, J., Sadok, W., Trugman, A. T., Williams, A. P., Wright, A. J., Abatzoglou, J. T., Dannenberg, M. P., Gentine, P., Guan, K., Johnston, M. R., Lowman, L. E. L., Moore, D. J. P., & McDowell, N. G. (2024). The impacts of rising vapour pressure deficit in natural and managed ecosystems. *Plant, Cell & Environment*, *47*(9), 3561–3589. https://doi.org/10.1111/pce.14846

Novick, K. A., Ficklin, D. L., Stoy, P. C., Williams, C. A., Bohrer, G., Oishi, A. C., Papuga, S. A., Blanken, P. D., Noormets, A., Sulman, B. N., Scott, R. L., Wang, L., & Phillips, R. P. (2016). The increasing importance of atmospheric demand for ecosystem water and carbon fluxes. *Nature Climate Change*, *6*(11), 1023–1027. https://doi.org/10.1038/nclimate3114

Oksanen, J., Simpson, G. L., Blanchet, F. G., Kindt, R., Legendre, P., Minchin, P. R., … & Weedon, J. (2013). Community ecology package. *R package version*, *2*(0), 321–326. https://doi.org/10.32614/CRAN.package.vegan

Pärn, J., Verhoeven, J. T. A., Butterbach-Bahl, K., Dise, N. B., Ullah, S., Aasa, A., … & Mander, Ü. (2018). Nitrogen-rich organic soils under warm well-drained conditions are global nitrous oxide emission hotspots. *Nature Communications*, *9*(1), 1135. https://doi.org/10.1038/s41467-018-03540-1

Peichl, M., Gažovič, M., Vermeij, I., De Goede, E., Sonnentag, O., Limpens, J., & Nilsson, M. B. (2018). Peatland vegetation composition and phenology drive the seasonal trajectory of maximum gross primary production. *Scientific Reports*, *8*(1), 8012. https://doi.org/10.1038/s41598-018-26147-4

Peng, J., Tang, J., Xie, S., Wang, Y., Liao, J., Chen, C., Sun, C., Mao, J., Zhou, Q., & Niu, S. (2024). Evidence for the acclimation of ecosystem photosynthesis to soil moisture. *Nature Communications*, *15*(1), 9795. https://doi.org/10.1038/s41467-024-54156-7

Penman, H. L. (1948). Natural evaporation from open water, bare soil and grass. *Proceedings of the Royal Society of London. Series A. Mathematical and Physical Sciences*, *193*(1032), 120–145.

Penman, H. L. (1956). Evaporation: an introductory survey. *Netherlands Journal of Agricultural Science*, *4*(1), 9–29.

Pereira, L. S., Allen, R. G., Smith, M., & Raes, D. (2015). Crop evapotranspiration estimation with FAO56: Past and future. *Agricultural Water Management*, *147*, 4–20. https://doi.org/10.1016/j.agwat.2014.07.031

Perez-Quezada, J. F., Trejo, D., Lopatin, J., Aguilera, D., Osborne, B., Galleguillos, M., Zattera, L., Celis-Diez, J. L., & Armesto, J. J. (2024). Comparison of carbon and water fluxes and the drivers of ecosystem water use efficiency in a temperate rainforest and a peatland in southern South America. *Biogeosciences*, *21*(5), 1371–1389. https://doi.org/10.5194/bg-21-1371-2024

Périé, C., & Ouimet, R. (2008). Organic carbon, organic matter and bulk density relationships in boreal forest soils. *Canadian Journal of Soil Science*, *88*(3), 315–325. https://doi.org/10.4141/CJSS06008

Petrescu, A. M. R., Lohila, A., Tuovinen, J.-P., Baldocchi, D. D., Desai, A. R., Roulet, N. T., … & Cescatti, A. (2015). The uncertain climate footprint of wetlands under human pressure. *Proceedings of the National Academy of Sciences*, *112*(15), 4594–4599. https://doi.org/10.1073/pnas.1416267112

Phoenix, G. K., & Bjerke, J. W. (2016). Arctic browning: Extreme events and trends reversing arctic greening. *Global Change Biology*, *22*(9), 2960–2962. https://doi.org/10.1111/gcb.13261

Poggio, L., De Sousa, L. M., Batjes, N. H., Heuvelink, G. B. M., Kempen, B., Ribeiro, E., & Rossiter, D. (2021). SoilGrids 2.0: Producing soil information for the globe with quantified spatial uncertainty. *Soil*, *7*(1), 217–240. https://doi.org/10.5194/soil-7-217-2021

Price, J. (1997). Soil moisture, water tension, and water table relationships in a managed cutover bog. *Journal of Hydrology*, *202*(1), 21–32. https://doi.org/10.1016/S0022-1694(97)00037-1

Qiu, C., Zhu, D., Ciais, P., Guenet, B., & Peng, S. (2020). The role of northern peatlands in the global carbon cycle for the 21st century. *Global Ecology and Biogeography*, *29*(5), 956–973. https://doi.org/10.1111/geb.13081

Quan, Q., Tian, D., Luo, Y., Zhang, F., Crowther, T. W., Zhu, K., Chen, H. Y. H., Zhou, Q., & Niu, S. (2019). Water scaling of ecosystem carbon cycle feedback to climate warming. *Science Advances*, *5*(8), eaav1131. https://doi.org/10.1126/sciadv.aav1131

Reichstein, M., Falge, E., Baldocchi, D., Papale, D., Aubinet, M., Berbigier, P., … & Valentini, R. (2005). On the separation of net ecosystem exchange into assimilation and ecosystem respiration: review and improved algorithm. *Global change biology*, *11*(9), 1424–1439. https://doi.org/10.1111/j.1365-2486.2005.001002.x

Running, S. W., & Zhao, M. (2015). Daily GPP and annual NPP (MOD17A2/A3) products NASA Earth Observing System MODIS land algorithm. *MOD17 User's Guide*, *2015*, 1–28.

Allen, R. G., Pereira, L. S., Raes, D., & Smith, M. (1998). Crop evapotranspiration–Guidelines for computing crop water requirements. *FAO Irrigation and drainage paper* 56. *FAO, Rome*, *300*(9), D05109.

Satriawan, T. W., Nyberg, M., Lee, S.-C., Christen, A., Black, T. A., Johnson, M. S., Nesic, Z., Merkens, M., & Knox, S. H. (2023). Interannual variability of carbon dioxide (CO_2) and methane (CH_4) fluxes in a rewetted temperate bog. *Agricultural and Forest Meteorology*, *342*, 109696. https://doi.org/10.1016/j.agrformet.2023.109696

Schwingshackl, C., Hirschi, M., & Seneviratne, S. I. (2017). Quantifying spatiotemporal variations of soil moisture control on surface energy balance and near-surface air temperature. *Journal of Climate*, *30*(18), 7105–7124. https://doi.org/10.1175/JCLI-D-16-0727.1

Seneviratne, S. I., Corti, T., Davin, E. L., Hirschi, M., Jaeger, E. B., Lehner, I., Orlowsky, B., & Teuling, A. J. (2010). Investigating soil moisture–climate interactions in a changing climate: A review. *Earth-Science Reviews*, *99*(3-4), 125–161. https://doi.org/10.1016/j.earscirev.2010.02.004

Silc, T., & Stanek, W. (1977). Bulk density estimation of several peats in northern Ontario using the von Post humification scale. *Canadian Journal of Soil Science*, *57*(1), 75–75.

Spawn, S. A., Sullivan, C. C., Lark, T. J., & Gibbs, H. K. (2020). Harmonized global maps of above and belowground biomass carbon density in the year 2010. *Scientific Data*, *7*(1), 112. https://doi.org/10.1038/s41597-020-0444-4

Stocker, B. D., Dong, N., Perkowski, E. A., Schneider, P. D., Xu, H., de Boer, H. J., Rebel, K. T., Smith, N. G., Van Sundert, K., Wang, H., Jones, S. E., Prentice, I. C., & Harrison, S. P. (2025). Empirical evidence and theoretical understanding of ecosystem carbon and nitrogen cycle interactions. *New Phytologist*, *245*(1), 49–68. https://doi.org/10.1111/nph.20178

Sugihara, G., Grenfell, B. T., May, R. M., & Tong, H. (1997). Nonlinear forecasting for the classification of natural time series. *Philosophical Transactions of the Royal Society of London. Series A: Physical and Engineering Sciences*, *348*(1688), 477–495. https://doi.org/10.1098/rsta.1994.0106

Sugihara, G., May, R., Ye, H., Hsieh, C., Deyle, E., Fogarty, M., & Munch, S. (2012). Detecting causality in complex ecosystems. *Science*, *338*(6106), 496–500. https://doi.org/10.1126/science.1227079

Takens, F. (1980). Detecting strange attractors in turbulence. In *Dynamical Systems and Turbulence, Warwick 1980: proceedings of a symposium held at the University of Warwick 1979/80* (pp. 366–381). Berlin, Heidelberg: Springer Berlin Heidelberg.

Taylor, P. G., Cleveland, C. C., Wieder, W. R., Sullivan, B. W., Doughty, C. E., Dobrowski, S. Z., & Townsend, A. R. (2017). Temperature and rainfall interact to control carbon cycling in tropical forests. *Ecology Letters*, *20*(6), 779–788. https://doi.org/10.1111/ele.12765

Thom, A. S. (1972). Momentum, mass and heat exchange of vegetation. *Quarterly Journal of the Royal Meteorological Society*, *98*(415), 124–134. https://doi.org/10.1002/qj.49709841510

Thompson, D. K., & Waddington, J. M. (2008). Sphagnum under pressure: Towards an ecohydrological approach to examining Sphagnum productivity. *Ecohydrology*, *1*(4), 299–308. https://doi.org/10.1002/eco.31

Tian, J., Branfireun, B. A., & Lindo, Z. (2020). Global change alters peatland carbon cycling through plant biomass allocation. *Plant and Soil*, *455*(1), 53–64. https://doi.org/10.1007/s11104-020-04664-4

Treat, C. C., Kleinen, T., Broothaerts, N., Dalton, A. S., Dommain, R., Douglas, T. A., … & Brovkin, V. (2019). Widespread global peatland establishment and persistence over the last 130,000 y. *Proceedings of the National Academy of Sciences*, *116*(11), 4822–4827. https://doi.org/10.1073/pnas.1813305116

Tschumi, E., Lienert, S., Van Der Wiel, K., Joos, F., & Zscheischler, J. (2022). The effects of varying drought–heat signatures on terrestrial carbon dynamics and vegetation composition. *Biogeosciences*, *19*(7), 1979–1993. https://doi.org/10.5194/bg-19-1979-2022

Turetsky, M. R., Benscoter, B., Page, S., Rein, G., van der Werf, G. R., & Watts, A. (2015). Global vulnerability of peatlands to fire and carbon loss. *Nature Geoscience*, *8*(1), 11–14. https://doi.org/10.1038/ngeo2325

Verma, S. B. (1989). Aerodynamic resistances to transfers of heat, mass and momentum.

Vicente-Serrano, S. M., Beguería, S., & López-Moreno, J. I. (2010a). A multiscalar drought index sensitive to global warming: The standardized precipitation evapotranspiration index. *Journal of Climate*, *23*(7), 1696–1718. https://doi.org/10.1175/2009JCLI2909.1

Vicente-Serrano, S. M., Beguería, S., López-Moreno, J. I., Angulo, M., & El Kenawy, A. (2010b). A new global 0.5 gridded dataset (1901–2006) of a multiscalar drought index: Comparison with current drought index datasets based on the Palmer Drought Severity Index. *Journal of Hydrometeorology*, *11*(4), 1033–1043. https://doi.org/10.1175/2010JHM1224.1

Vlachos, I., & Kugiumtzis, D. (2009). State space reconstruction from multiple time series. In *Topics on Chaotic Systems: Selected Papers from Chaos 2008 International Conference* (pp. 378–387). https://doi.org/10.1142/9789814271349_0043

Voigt, C., Dubbert, M., Launiainen, S., Porada, P., Oestmann, J., & Piayda, A. (2024). Impact of vegetation composition and seasonality on sensitivity of modelled CO_2 exchange in temperate raised bogs. *Scientific Reports*, *14*(1), 11023. https://doi.org/10.1038/s41598-024-61229-6

von Post, L., & Granlund, E. (1926). *Södra Sveriges torvtillgångar*. Sveriges Geologiska Undersökning, Stockholm.

Wang, H., Richardson, C. J., & Ho, M. (2015). Dual controls on carbon loss during drought in peatlands. *Nature Climate Change*, *5*(6), 584–587. https://doi.org/10.1038/nclimate2643

Wang, H., Yan, S., Ciais, P., Wigneron, J.-P., Liu, L., Li, Y., Fu, Z., Ma, H., Liang, Z., Wei, F., Wang, Y., & Li, S. (2022). Exploring complex water stress–gross primary production relationships: Impact of climatic drivers, main effects, and interactive effects. *Global Change Biology*, *28*(13), 4110–4123. https://doi.org/10.1111/gcb.16201

Wang, L., Zhu, H., Lin, A., Zou, L., Qin, W., & Du, Q. (2017). Evaluation of the latest MODIS GPP products across multiple biomes using global eddy covariance flux data. *Remote Sensing*, *9*(5), 418. https://doi.org/10.3390/rs9050418

Wang, Y., Hao, Y., Cui, X. Y., Zhao, H., Xu, C., Zhou, X., & Xu, Z. (2014). Responses of soil respiration and its components to drought stress. *Journal of Soils and Sediments*, *14*(1), 99–109. https://doi.org/10.1007/s11368-013-0799-7

Watts, J. D., Natali, S. M., Minions, C., Risk, D., Arndt, K., Zona, D., Euskirchen, E. S., Rocha, A. V., Sonnentag, O., Helbig, M., Kalhori, A., Oechel, W., Ikawa, H., Ueyama, M., Suzuki, R., Kobayashi, H., Celis, G., Schuur, E. A. G., Humphreys, E., … Edgar, C. (2021). Soil respiration strongly offsets carbon uptake in Alaska and Northwest Canada. *Environmental Research Letters*, *16*(8), 084051. https://doi.org/10.1088/1748-9326/ac1222

Weiss, R., Alm, J., Laiho, R., & Laine, J. (1998). Modeling moisture retention in peat soils. *Soil Science Society of America Journal*, *62*(2), 305–313. https://doi.org/10.2136/sssaj1998.03615995006200020002x

Weltzin, J. F., Pastor, J., Harth, C., Bridgham, S. D., Updegraff, K., & Chapin, C. T. (2000). Response of bog and fen plant communities to warming and water-table manipulations. *Ecology*, *81*(12), 3464–3478. https://doi.org/10.1890/0012-9658(2000)081[3464:ROBAFP]2.0.CO;2

Wilkinson, S. L., Andersen, R., Moore, P. A., Davidson, S. J., Granath, G., & Waddington, J. M. (2023). Wildfire and degradation accelerate northern peatland carbon release. *Nature Climate Change*, *13*(5), 456–461. https://doi.org/10.1038/s41558-023-01657-w

Williams, M., Schwarz, P. A., Law, B. E., Irvine, J., & Kurpius, M. R. (2005). An improved analysis of forest carbon dynamics using data assimilation. *Global Change Biology*, *11*(1), 89–105. https://doi.org/10.1111/j.1365-2486.2004.00891.x

Williams, T. G., & Flanagan, L. B. (1996). Effect of changes in water content on photosynthesis, transpiration and discrimination against $^{13}CO_2$ and $C^{18}O^{16}O$ in *Pleurozium* and *Sphagnum*. *Oecologia*, *108*(1), 38–46. https://doi.org/10.1007/BF00333212

Wutzler, T., & Carvalhais, N. (2014). Balancing multiple constraints in model–data integration: Weights and the parameter block approach. *Journal of Geophysical Research: Biogeosciences*, *119*(11), 2112–2129. https://doi.org/10.1002/2014JG002650

Wyatt, K. H., Turetsky, M. R., Rober, A. R., Giroldo, D., Kane, E. S., & Stevenson, R. J. (2012). Contributions of algae to GPP and DOC production in an Alaskan fen: Effects of historical water table manipulations on ecosystem responses to a natural flood. *Oecologia*, *169*(3), 821–832. https://doi.org/10.1007/s00442-011-2233-4

Yavitt, J. B., Williams, C. J., & Wieder, R. K. (1997). Production of methane and carbon dioxide in peatland ecosystems across North America: Effects of temperature, aeration, and organic chemistry of peat. *Geomicrobiology Journal*, *14*(4), 299–316. https://doi.org/10.1080/01490459709378054

Ye, H., Beamish, R. J., Glaser, S. M., Grant, S. C. H., Hsieh, C., Richards, L. J., Schnute, J. T., & Sugihara, G. (2015). Equation-free mechanistic ecosystem forecasting using empirical dynamic modeling. *Proceedings of the National Academy of Sciences*, *112*(13), E1569–E1576. https://doi.org/10.1073/pnas.1417063112

Yu, Z. (2011). Holocene carbon flux histories of the world's peatlands: Global carboncycle implications. *The Holocene*, *21*(5), 761–774. https://doi.org/10.1177/0959683610386982

Yu, Z., Loisel, J., Brosseau, D. P., Beilman, D. W., & Hunt, S. J. (2010). Global peatland dynamics since the Last Glacial Maximum. *Geophysical Research Letters*, *37*(13). https://doi.org/10.1029/2010GL043584

Zarakas, C. M., Swann, A. L., Laguë, M. M., Armour, K. C., & Randerson, J. T. (2020). Plant physiology increases the magnitude and spread of the transient climate response to CO_2 in CMIP6 Earth system models. *Journal of Climate*, *33*(19), 8561–8578. https://doi.org/10.1175/JCLI-D-20-0078.1

Zhang, Y., Xiao, X., Zhou, S., Ciais, P., McCarthy, H., & Luo, Y. (2016). Canopy and physiological controls of GPP during drought and heat wave. *Geophysical Research Letters*, *43*(7), 3325–3333. https://doi.org/10.1002/2016GL068501

SUMMARY

Global warming, intensity, and frequency of extreme climatic events (droughts, wildfires, extreme heat, extreme precipitation, etc.) are projected to increase. It is expected to be driven by land use and land cover change (LULCC) and resulting greenhouse gas (GHG) emissions. Peatlands play a crucial role in the global carbon (C) and GHG budget by accumulating carbon (C) in soils (more than the global terrestrial vegetation). Saturated peat soils reduce decomposition and create an imbalance between gross primary productivity (GPP) and ecosystem respiration (Reco; i.e. heterotrophic respiration and autotrophic respiration). Soil water balance, movement of water in the soil–plant–atmosphere continuum, and meteorological drivers of GPP (shortwave radiation, atmospheric water demand: i.e. vapour pressure deficit (VPD), air temperature, and precipitation) are of the utmost importance for the ecosystem, regional, and global C and other GHG balance. Post-industrial revolution peatland land-use and land-cover change (LULCC) and resulting global warming have diverse and dire negative impacts on C and other GHG balances. Peatland drainage and water table drawback cause peat oxidation, leading to CO_2 through heterotrophic respiration (microbial respiration). Increased microbial activity can lead to N_2O emissions. Empirical knowledge of how soil moisture variations impact soil GHG emissions is essential for reducing the uncertainty around the process-based understanding of peatland ecosystems (Articles I and II). These changes shift peatlands to be a source of CO_2 further amplifying the global warming effect. Increased atmospheric GHG blocks more solar radiation reflected from the earth's surface to space, increasing temperature, VPD, etc. For example, an increase in VPD and temperature could lead to atmospheric drought as there may not be enough water in the soil to evaporate to meet the demand. Such an event could lead to a decline in GPP (negative climate-carbon feedback). It necessitates the knowledge of GPP-VPD-SWC dynamics (Article IV). On the other hand, the rise in atmospheric CO_2 can also cause climate-carbon feedback known as CO_2 fertilisation effect (A growth in photosynthesis due to increased availability of atmospheric CO_2 given there are no limiting factors such as soil moisture, shortwave radiation, air temperature). This may cause changes to C allocation (to different plant tissues) patterns and C residence times (Amount of time C spends in plant tissues/pools) (Article III). Articles I and II use a statistical regression modelling approach to investigate soil GHG dynamics and its key biotic and abiotic drivers across 48 open peatlands between the 2011 and 2020 growing seasons. Each site constitutes 4 to 6 days of field campaigning for chamber-based gas measurements and soil samples for physical and chemical analysis. Results showed GHG and net ecosystem exchange (NEE) had a Gaussian (unimodal) relationship with soil moisture, a finding that contradicts the current knowledge (positive linear relationship of GHG and, more specifically, CO_2 fluxes with soil moisture). This means that sites with intermediate soil moisture (40% to 65% of the pore space) were sources of GHG (i.e. emissions). Net ecosystem exchange (NEE) was the most

prevalent in GHG emissions. Microbial abundance explained the remaining variations in GHG dynamics. Microbial abundance was driven by C:N ratio.

Article III and IV focus on land-atmosphere exchange of CO_2, its drivers, and ecosystem-scale responses. Articles I and II found CO_2 was predominant in GHG exchange. It specifically investigates the two climate–carbon feedbacks mentioned above. Specifically, Article III highlights the positive climate–carbon feedback of CO_2 fertilisation in a sub-Arctic fen peatland in Alaska, USA. This study employs an intermediate terrestrial ecosystem model of C called the Data Assimilation Linked Ecosystem Carbon version 2 (DALEC2) model. DALEC2 was calibrated using a Bayesian approach called carbon model data fusion framework (CARDAMOM). Publicly available weekly time step eddy covariance data (2014 to 2020), along with in-situ measurements, were used to calibrate the model. Additional synthetic experiments on the calibrated DALEC model and photosynthetic sub-model aggregated canopy model version 1 (ACM1) were used to determine CO_2 fertilisation effect, its direct, and indirect effect on GPP, respectively. Experiments on calibrated DALEC models, namely fixed CO_2 experiment and fixed climate experiment, showed that CO_2 fertilisation (rather than other meteorological drivers such as air temperature, shortwave radiation, and precipitation) was behind the GPP growth seen in the CARDAMOM results. Experiments with the ACM1 sub-model implied that 4% of the increase in GPP was the indirect cause of leaf area growth as the result of CO_2 fertilisation. Moreover, this study was able to show ecosystem scale rates of photosynthate allocation to different plant tissues, their residence time and total C stock in different biomass pools. Results show that the foliage C pool was favoured over fine root and structural C pools. Furthermore, while foliage C had a residence time of 6 months, fine root C had a residence time of 4.5 years. To my knowledge, this is the first study to show these internal C traits at an ecosystem scale. Article IV investigates negative climate-carbon feedback caused by atmospheric drought. A causal inference approach called empirical dynamic modelling (EDM) was combined with a model that tracks water movement through the soil-plant-atmosphere continuum. The ecophysiological model is based on the "big leaf" assumption. i.e. vegetation is represented as a single uniform layer/one large canopy. Additionally, drought was determined using the standard precipitation evapotranspiration index in combi- nation with the moisture index. These models showed that during the first severe drought of 2016, GPP was limited by VPD and other energy-related drivers (short- wave radiation and air temperature) through stomatal regulation (plants chose water retention over C assimilation). In the next two years (2017 and 2018), due to the absence of severe drought, plants maximised C assimilation (hence the relatively high GPP observed in the data). Nevertheless, it caused water table drawdown to –8cm (soil moisture of 82.5%) by 2019, causing the GPP to be limited by soil moisture. In this article, the threshold at which soil moisture limits GPP is identified as 82.5% of pore space. Causal inference corroborates the findings. The causal effect of VPD and energy-related drivers was higher than that of soil moisture and water table depth on GPP in all the years except 2019.

SUMMARY IN ESTONIAN

Soode süsiniku- ja lämmastikuvoogude modelleerimine ökosüsteemi tasandil

Maakera kliima soojeneb ja äärmuslikud ilmasündmused sagenevad. Seda põhjustavad maakasutuse ja maakatte muutused ning nendest tulenevad kasvuhoonegaaside (KHG) heitmed. Sood mängivad olulist rolli globaalses süsiniku ja kasvuhoonegaaside bilansis, salvestades süsinikku mulda. Mullasüsinikku on maakeral rohkem kui maismaa taimestikus. Täpsemalt väheneb märjas mullas orgaanika lagunemine, mis kallutab taimekasvu ja ökosüsteemi hingamise vahelise bilansi süsiniku salvestamise poole. Selle tagajärjel tekib turvasmuld. Süsihappegaasi (CO_2) ja teiste KHG-de vahekorra kujunemisel on olulised mulla veebilanss, vee liikumine muld–taim–atmosfäär süsteemis ning taimekasvu mõjutavad ilmategurid (lühilainekiirgus, atmosfääri niiskusvajak, õhutemperatuur ja sademed). Tööstusrevolutsiooni järgsel ajastul toimunud soode muutused ning nendest tulenev globaalne soojenemine on KHG bilansile avaldanud tõsiselt negatiivset mõju. Soode kuivendamine põhjustab turba oksüdeerumist, mis viib CO_2 lendumisele heterotroofse (st. mikroobide) hingamise kaudu. Suurenenud mikroobide aktiivsus võib põhjustada naerugaasi (N_2O) emissiooni. Teadmine sellest, kuidas mullaniiskuse muutused mõjutavad mulla KHG heitmeid, on oluline, et mõista soo-ökosüsteemides toimuvaid protsesse ka laiemalt (artiklid I ja II). Need muutused viivad sood CO_2 sidujatest selle allikateks, suurendades globaalset soojenemist veelgi. Kliima soojenemine tõstab ka niiskusvajakut ja tekitada atmosfääris äärmist kuivust, mis vähendab taimekasvu. Nende tegurite ühine analüüs aitab paremini mõista taimekasvu ja niiskustegurite kompleksi dünaamikat (artikkel IV). Vastupidise st. negatiivse tagasiside tekitab CO_2 väetamisefekt, milles atmosfääri CO_2 kättesaadavuse soodustab taimekasvu. See võib põhjustada muutusi süsiniku jaotumises taimestiku ja ökosüsteemi erinevatesse osadesse ning süsiniku viibeajas (artikkel III). Artiklites I and II tekitati statistilisi regressioonimudelit, iseloomustamaks KHG dünaamikat ja nende peamisi tegureid maakera lagesoode temperatuuri, niiskuse, toitainete sisalduse ja maakasutuse tunnusruumis. Andmed pärinevad ajavahemikul 2011–2020 tehtud 48 lagesoo kambrimeetodil KHG voogude mõõtmistest ning mullaproovide füüsikaliste ja keemiliste parameetrite analüüsist. Tulemused näitasid, et KHG heitmed oli kõrgeimad mõõdukal mullaniiskusel. See tulemus seab kahtluse alla praegust teadmist lineaarse seose kohta CO_2 heitme ja mullaniiskuse vahel. CO_2 vood olidki KHG-bilansi kaalukaim osa. Sel põhjusel keskendusid artiklid III ja IV maismaa ja atmosfääri CO_2 vahetusele jamõjuritele. Artikkel III analüüsis CO_2 väetamisefekti Alaska lähisarktilises madalsoos. Uuring kasutas keskmise keerukusega maismaaökosüsteemi mudelit nimega DALEC2. Mudelit kalibreeriti Bayesi meetodil CARDAMOM abimudeliga. Kalibreerimiseks kasutati turbulentse õhuvoo mõõtmiste avaandmeid (2014.–2020.a.) ning ka maa-

pealseid kambrimõõtmisi. CO_2 väetamisefekti kontrolliti kalibreeritud DALEC mudeli ja fotosünteesi alam-mudeli (ACM1) keskkonnas läbiviidud katsetega. Kummaski katses fikseeriti vastavalt kas CO_2 või ilmanäitajad. Katsetulemus näitas, et just CO_2 väetamise mõju, mitte ilmanäitajad, olid CARDAMOMi tulemustes nähtud taimekasvu tõusu taga. Saadud 4% taimekasvu tõus korreleerus kaugseire abil tuvastatud lehepinna-indeksi tõusuga. Lisaks näitas uuring ära taimekasvu saaduste jaotumist ökosüsteemi osadesse, nende viibeaega ja vastvavate süsinikuvarude muutumist. Peamiselt liikus süsinik lehtedesse mitte peenjuurtesse ega struktuursesse süsinikuvarusse. Lehesüsiniku viibeaeg oli 6 kuud, peenjuurte süsinikul 4,5 aastat. Teadaolevalt on see esimene uuring, mis näitab süsiniku jaotumist soo-ökosüsteemi osades. Artikkel IV uuris põua ja süsinikuvoogude vahelist tagasisidet. Seoste põhjuslikkuse tuvastamise meetodit, mida nimetatakse empiirilis-dünaamiliseks modelleerimiseks (EDM), kasutati koos mudeliga, mis jälgib vee liikumist muld–taim–atmosfäär süsteemis. Ökofüsioloogiline mudel põhineb nn. „suure lehe“ lihtsustusel, mis taandab taimestiku ühele kujuteldavale lehekihile. Põud määratleti sademete ja aurumise indeksi ning niiskus-indeksi kombinatsioonis. Mudelid näitasid, et 2016. a. põua ajal limiteerisid taimekasvu õhuniiskuse vajaku ja soojusenergia kättesaadavusega seotud tegurid nagu lühilainekiirgus ja õhutemperatuur. Põua ajal sulgesid taimed õhulõhed, valides fotosünteesi asemel veevaru säilitamise. Põuale järgnenud kahel aastal (2017. ja 2018.a.), mil atmosfääris oli piisavalt niiskust, maksimeerisid taimed fotosünteesi ja seega primaarproduktsiooni. Järgnenud 2019. aastal langes põhjaveetase 8cm sügavusele maapinnast (mullaniiskus 82,5%), mis võis taimekasvu piirata. Seoste põhjuslikkuse analüüs kinnitas neid tulemusi.

ACKNOWLEDGEMENTS

I express sincere gratitude to my supervisory team of Asso. Prof. Jaan Pärn, Prof. Ülo Mander, and Dr. Thomas Luke Smallman. This PhD journey would not have been possible without their unwavering support. I thank Jaan and Ülo for providing opportunity to join the team. I thank Prof Mathew Williams (School of GeoSciences, The University of Edinburgh, UK) for accepting me as a visiting PhD student to Global Change Ecology Lab (GCEL). Edinburgh visit played a vital role in shaping my PhD. I will always be grateful to Jaan, Ülo, Luke and Mat for the patience they have shown. I would like to thank collaborators Eugénie S Euskirchen, Evan S Kane, Sara H Knox, and June Skeeter for their contribution to my research. I express gratitude to my parents for their support and sacrifices. I would like to thank friends and colleagues Sharvari Gadegaonkar, Tim Green, David Mildowski, Matus Seci, and Nina Fischer, Mohit Masta, Fahad Ali Kazmi, Arun Kumar Devarajan, Kapil Raj Periyasammi, Keerthana Chithanathan, and Sudhichan Mehta for their camaraderie and helpful discussions and comments during this journey.

The studies included in this thesis were supported by the following grants and funding agencies. The Dora Plus activity 1.2 “PhD student mobility” scholarship through European Regional Development Fund, Erasmus+ student mobility for PhD traineeship, the Estonian Research Council (grants PRG-352 and PRG2032), European Commission through the HORIZON-WIDERA “Living Labs for Wetland Forest Research” Twinning project No 101079192, European Research Council (ERC) under the grant agreement No 101096403 (MLTOM23415R), and the European Regional Development Fund (Centre of Excellence EcolChange, grant number TK-131 and Centre of Excellence AgroCropFuture; TK-200). The field data collected for Article III was funded by the National Science Foundation Grants DEB LTREB 1354370 and 2011257, DEB-0425328, DEB-0724514, and DEB-0830997. The Bonanza Creek Long Term Experimental Research station provided lab space, equipment, and time to the project. Research equipment for Article IV is funded through research contracts between Metro Vancouver and UBC (PI: Knox). Selected equipment was supported by the Canada Foundation for Innovation (Christen, Johnson, and Knox; project number 39738).

PUBLICATIONS

CURRICULUM VITAE

Name: Sandeep Thayamkottu
Date of birth: 27.08.1994
Citizenship: India
E-mail: sandeep.thayamkottu@ut.ee

Education

Ph.D. Physical Geography
University of Tartu 2020 –

Master of Science in Geoinformatics
Cochin University of Science and Technology 2015 – 2017

Bachelor of Science
University of Calicut 2012–2015

Research experience

Junior research fellow
University of Tartu 2022–

Visiting Ph.D. student
The University of Edinburgh 2022 October–2023 March

Research project fellow
Indian Institute of Space Science and Technology 2018–2020

Research assistant
Kerala Forest Research Institute December 2017 – March 20218

Research interests

carbon and water cycle coupling in the soil–plant–atmosphere continuum, model–data integration, remote sensing, eddy covariance, machine learning, extreme events

Scholarships

Erasmus+ Ph.D. trainee grant
European Commission, January 2023 – March 2023
Scholarship to cover the secondment to the Global Change Ecology Lab, The University of Edinburgh

Dora+ long-term Ph.D. mobility fellowship
The Estonian Education & Youth Board through the European Regional Development Fund
2022 October – December 2022
Awarded for funding the PhD mobility to the University of Edinburgh

Performance stipend
University of Tartu, 2020–2024

Doctoral allowance
University of Tartu, 2020–2024

Publications (including manuscripts under revision)

Kazmi, F. A., Espenberg, M., Pärn, J., Masta, M., Ranniku, R., **Thayamkottu, S**., & Mander, Ü. (2025). Meltwater of freeze-thaw cycles drives N_2O-governing microbial communities in a drained peatland forest soil. *Biology and Fertility of Soils, 61*(3), 667–680. https://doi.org/10.1007/s00374-023-01790-w

Masta, M., Espenberg, M., Kuusemets, L., Pärn, J., **Thayamkottu, S.,** Sepp, S., Kirsimäe, K., Sgouridis, F., Kasak, K., Soosaar, K., & Mander, Ü. (2024). ^{15}N tracers and microbial analyses reveal in situ N_2O sources in contrasting water regimes of a drained peatland forest. *Pedosphere, 34*(4), 749–758. https://doi.org/10.1016/j.pedsph.2023.06.006

Pärn, J., Espenberg, M., Soosaar, K., Kasak, K., **Thayamkottu, S.,** Schindler, T., Ranniku, R., Sohar, K., Fachín Malaverri, L., Melling, L., & Mander, Ü. Importance of N_2O in greenhouse gas budgets of tropical peatlands. *Submitted*.

Pärn, J., **Thayamkottu, S.,** Öpik, M., Bahram, M., Tedersoo, L., Espenberg, M., Davison, J. A., Kasak, K., Maddison, M., Niinemets, Ü., Ostonen, I., Soosaar, K., Zobel, M., & Mander, Ü. (2025). Soil moisture and microbiome explain greenhouse gas exchange in global peatlands. *Scientific Reports, 15*(1), 10153. https://doi.org/10.1038/s41598-025-92891-z

Thayamkottu, S., Masta, M., Skeeter, J., Pärn, J., Knox, S. H., & Mander, Ü. (2025). Dual controls of vapour pressure deficit and soil moisture on photosynthesis in a restored temperate bog. *Science of the Total Environment, 963*, 178366. https://doi.org/10.1016/j.scitotenv.2024.178366

Thayamkottu, S., & Joseph, S. (2018). Tropical forest cover dynamics and carbon emissions-contribution of remote sensing and data mining techniques. *Tropical Ecology, 59*(4), 555–563.

Thayamkottu, S., Smallman, T. L., Pärn, J., Mander, Ü., Euskirchen, E. S., & Kane, E. S. (2024). Greening of a boreal rich fen driven by CO_2 fertilisation. *Agricultural and Forest Meteorology, 359*, 110261. https://doi.org/10.1016/j.agrformet.2024.110261

ELULOOKIRJELDUS

Nimi: Sandeep Thayamkottu
Sünniaeg: 27.08.1994
Kodakondsus: India
E-post: sandeep.thayamkottu@ut.ee

Haridus

Doktoriõpe (*Ph.D*). loodusgeograafias
Tartu Ülikool, 2020–2025
Väitekirja pealkiri: "Soode süsiniku- ja lämmastikuvoogude modelleerimine ökosüsteemi tasandil"
Juhendajad: kaasprof. Jaan Pärn, prof. Ülo Mander ja dr. Thomas Luke Smallman

Magistrikraad geoinformaatikas
Cochini Teaduse ja Tehnoloogia Ülikool, 2015–2017

Bakalaureusekraad matemaatikas
Calicuti Ülikool, 2012–2015

Teenistuskäik

Nooremteadur
Tartu Ülikool, november 2022 –

Külalisdoktorant
Edinburghi Ülikool, globaalmuutuste ökoloogia labor
Juhendajad: prof Mathew Williams ja dr T Luke Smallman
oktoober 2022 – märts 2023

Teadusprojekti täitja

India kosmoseteaduse ja tehnoloogia instituut aprill 2018 – märts 2020

Assistent
Kerala Metsainstituut, detsember 2017 – märts 2018

Rahastus

Erasmus+ erialapraktikandi stipendium doktoriõppes
Euroopa Komisjon, jaanuar 2023 – märts 2023
Edinburghi ülikooli globaalmuutuste ökoloogia labori külastus

Dora+ pikaajaline doktorikraadi õpirände stipendium
Haridus- ja Noorsooamet Euroopa Regionaalarengu Fondi kaudu,
oktoober – detsember 2022 – Edinburghi Ülikooli külastus

Tulemusstipendium
Tartu Ülikool, 2020–2024

Doktoriõppe toetus
Tartu Ülikool, 2020–2024

Uurimissuunad

Aineringed, süsiniku ja veeringe muld–taim–atmosfääri kontiinumis, mudeliandmete integreerimine, kaugseire, masinõpe, ekstreemsed ilmanähtused

Publikatsioonid (sealhulgas eelretsenseerimisel käsikirjad)

Kazmi, F. A., Espenberg, M., Pärn, J., Masta, M., Ranniku, R., **Thayamkottu, S**., & Mander, Ü. (2025). Meltwater of freeze-thaw cycles drives N_2O-governing microbial communities in a drained peatland forest soil. *Biology and Fertility of Soils, 61*(3), 667–680. https://doi.org/10.1007/s00374-023-01790-w

Masta, M., Espenberg, M., Kuusemets, L., Pärn, J., **Thayamkottu, S.,** Sepp, S., Kirsimäe, K., Sgouridis, F., Kasak, K., Soosaar, K., & Mander, Ü. (2024). ^{15}N tracers and microbial analyses reveal in situ N_2O sources in contrasting water regimes of a drained peatland forest. *Pedosphere, 34*(4), 749–758. https://doi.org/10.1016/j.pedsph.2023.06.006

Pärn, J., Espenberg, M., Soosaar, K., Kasak, K., **Thayamkottu, S.,** Schindler, T., Ranniku, R., Sohar, K., Fachín Malaverri, L., Melling, L., & Mander, Ü. Importance of N_2O in greenhouse gas budgets of tropical peatlands. *Submitted.*

Pärn, J., **Thayamkottu, S.,** Öpik, M., Bahram, M., Tedersoo, L., Espenberg, M., Davison, J. A., Kasak, K., Maddison, M., Niinemets, Ü., Ostonen, I., Soosaar, K., Zobel, M., & Mander, Ü. (2025). Soil moisture and microbiome explain greenhouse gas exchange in global peatlands. *Scientific Reports, 15*(1), 10153. https://doi.org/10.1038/s41598-025-92891-z

Thayamkottu, S., Masta, M., Skeeter, J., Pärn, J., Knox, S. H., & Mander, Ü. (2025). Dual controls of vapour pressure deficit and soil moisture on photosynthesis in a restored temperate bog. *Science of the Total Environment, 963*, 178366. https://doi.org/10.1016/j.scitotenv.2024.178366

Thayamkottu, S., & Joseph, S. (2018). Tropical forest cover dynamics and carbon emissions-contribution of remote sensing and data mining techniques. *Tropical Ecology, 59*(4), 555–563.

Thayamkottu, S., Smallman, T. L., Pärn, J., Mander, Ü., Euskirchen, E. S., & Kane, E. S. (2024). Greening of a boreal rich fen driven by CO_2 fertilisation. *Agricultural and Forest Meteorology, 359*, 110261. https://doi.org/10.1016/j.agrformet.2024.110261

DISSERTATIONES GEOGRAPHICAE UNIVERSITATIS TARTUENSIS

1. **Вийви Руссак.** Солнечная радиация в Тыравере. Тарту, 1991.
2. **Urmas Peterson.** Studies on Reflectance Factor Dynamics of Forest Communities in Estonia. Tartu, 1993.
3. **Ülo Suursaar.** Soome lahe avaosa ja Eesti rannikumere vee kvaliteedi analüüs. Tartu, 1993.
4. **Kiira Aaviksoo.** Application of Markov Models in Investigation of Vegetation and Land Use Dynamics in Estonian Mire Landscapes. Tartu, 1993.
5. **Kjell Weppling.** On the assessment of feasible liming strategies for acid sulphate waters in Finland. Tartu, 1997.
6. **Hannes Palang.** Landscape changes in Estonia: the past and the future. Tartu, 1998.
7. **Eiki Berg.** Estonia's northeastern periphery in politics: socio-economic and ethnic dimensions. Tartu, 1999.
8. **Valdo Kuusemets.** Nitrogen and phosphorus transformation in riparian buffer zones of agricultural landscapes in Estonia. Tartu, 1999.
9. **Kalev Sepp.** The methodology and applications of agricultural landscape monitoring in Estonia. Tartu, 1999.
10. **Rein Ahas.** Spatial and temporal variability of phenological phases in Estonia. Tartu, 1999.
11. **Эркки Таммиксаар.** Географические аспекты творчества Карла Бэра в 1830–1840 гг. Тарту, 2000.
12. **Garri Raagmaa.** Regional identity and public leaders in regional economic development. Tartu, 2000.
13. **Tiit Tammaru.** Linnastumine ja linnade kasv Eestis nõukogude aastatel. Tartu, 2001.
14. **Tõnu Mauring.** Wastewater treatment weltlands in Estonia: efficiency and landscape analysis. Tartu, 2001.
15. **Ain Kull.** Impact of weather and climatic fluctuations on nutrient flows in rural catchments. Tartu, 2001.
16. **Robert Szava-Kovats.** Assessment of stream sediment contamination by median sum of weighted residuals regression. Tartu, 2001.
17. **Heno Sarv.** Indigenous Europeans east of Moscow. Population and Migration Patterns of the Largest Finno-Ugrian Peoples in Russia from the 18th to the 20th Centuries. Tartu, 2002.
18. **Mart Külvik.** Ecological networks in Estonia — concepts and applications. Tartu, 2002.
19. **Arvo Järvet.** Influence of hydrological factors and human impact on the ecological state of shallow Lake Võrtsjärv in Estonia. Tartu, 2004.
20. **Katrin Pajuste.** Deposition and transformation of air pollutants in coniferous forests. Tartu, 2004.

21. **Helen Sooväli.** *Saaremaa waltz*. Landscape imagery of Saaremaa Island in the 20th century. Tartu, 2004.
22. **Antti Roose.** Optimisation of environmental monitoring network by integrated modelling strategy with geographic information system — an Estonian case. Tartu, 2005.
23. **Anto Aasa.** Changes in phenological time series in Estonia and Central and Eastern Europe 1951–1998. Relationships with air temperature and atmospheric circulation. Tartu, 2005.
24. **Anneli Palo.** Relationships between landscape factors and vegetation site types: case study from Saare county, Estonia. Tartu, 2005.
25. **Mait Sepp.** Influence of atmospheric circulation on environmental variables in Estonia. Tartu, 2005.
26. **Helen Alumäe.** Landscape preferences of local people: considerations for landscape planning in rural areas of Estonia. Tartu, 2006.
27. **Aarne Luud.** Evaluation of moose habitats and forest reclamation in Estonian oil shale mining areas. Tartu, 2006.
28. **Taavi Pae.** Formation of cultural traits in Estonia resulting from historical administrative division. Tartu, 2006.
29. **Anneli Kährik.** Socio-spatial residential segregation in post-socialist cities: the case of Tallinn, Estonia. Tartu, 2006.
30. **Dago Antov.** Road user perception towards road safety in Estonia. Tartu, 2006.
31. **Üllas Ehrlich.** Ecological economics as a tool for resource based nature conservation management in Estonia. Tartu, 2007.
32. **Evelyn Uuemaa.** Indicatory value of landscape metrics for river water quality and landscape pattern. Tartu, 2007.
33. **Raivo Aunap.** The applicability of gis data in detecting and representing changes in landscape: three case studies in Estonia. Tartu, 2007.
34. **Kai Treier.** Trends of air pollutants in precipitation at Estonian monitoring stations. Tartu, 2008.
35. **Kadri Leetmaa.** Residential suburbanisation in the Tallinn metropolitan area. Tartu, 2008.
36. **Mare Remm.** Geographic aspects of enterobiasis in Estonia. Tartu, 2009.
37. **Alar Teemusk.** Temperature and water regime, and runoff water quality of planted roofs. Tartu, 2009.
38. **Kai Kimmel.** Ecosystem services of Estonian wetlands. Tartu, 2009.
39. **Merje Lesta.** Evaluation of regulation functions of rural landscapes for the optimal siting of treatment wetlands and mitigation of greenhouse gas emissions. Tartu, 2009.
40. **Siiri Silm.** The seasonality of social phenomena in Estonia: the location of the population, alcohol consumption and births. Tartu, 2009.
41. **Ene Indermitte.** Exposure to fluorides in drinking water and dental fluorosis risk among the population of Estonia. Tartu, 2010.
42. **Kaido Soosaar.** Greenhouse gas fluxes in rural landscapes of Estonia. Tartu, 2010.

43. **Jaan Pärn.** Landscape factors in material transport from rural catchments in Estonia. Tartu, 2010.
44. **Triin Saue.** Simulated potato crop yield as an indicator of climate variability in Estonia. Tartu, 2011.
45. **Katrin Rosenvald.** Factors affecting EcM roots and rhizosphere in silver birch stands. Tartu, 2011.
46. **Ülle Marksoo.** Long-term unemployment and its regional disparities in Estonia. Tartu, 2011, 163 p.
47. **Hando Hain.** The role of voluntary certification in promoting sustainable natural resource use in transitional economies. Tartu, 2012, 180 p.
48. **Jüri-Ott Salm.** Emission of greenhouse gases CO_2, CH_4, and N_2O from Estonian transitional fens and ombrotrophic bogs: the impact of different land-use practices. Tartu, 2012, 125 p.
49. **Valentina Sagris.** Land Parcel Identification System conceptual model: development of geoinfo community conceptual model. Tartu, 2013, 161 p.
50. **Kristina Sohar.** Oak dendrochronology and climatic signal in Finland and the Baltic States. Tartu, 2013, 129 p.
51. **Riho Marja.** The relationships between farmland birds, land use and landscape structure in Northern Europe. Tartu, 2013, 134 p.
52. **Olle Järv.** Mobile phone based data in human travel behaviour studies: New insights from a longitudinal perspective. Tartu, 2013, 168 p.
53. **Sven-Erik Enno.** Thunderstorm and lightning climatology in the Baltic countries and in northern Europe. Tartu, 2014, 142 p.
54. **Kaupo Mändla.** Southern cyclones in northern Europe and their influence on climate variability. Tartu, 2014, 142 p.
55. **Riina Vaht.** The impact of oil shale mine water on hydrological pathways and regime in northeast Estonia. Tartu, 2014, 111 p.
56. **Jaanus Veemaa.** Reconsidering geography and power: policy ensembles, spatial knowledge, and the quest for consistent imagination. Tartu, 2014, 163 p.
57. **Kristi Anniste.** East-West migration in Europe: The case of Estonia after regaining independence. Tartu, 2014, 151 p.
58. **Piret Pungas-Kohv.** Between maintaining and sustaining heritage in landscape: The examples of Estonian mires and village swings. Tartu, 2015, 210 p.
59. **Mart Reimann.** Formation and assessment of landscape recreational values. Tartu, 2015, 127 p.
60. **Järvi Järveoja.** Fluxes of the greenhouse gases CO_2, CH_4 and N_2O from abandoned peat extraction areas: Impact of bioenergy crop cultivation and peatland restoration. Tartu, 2015, 171 p.
61. **Raili Torga.** The effects of elevated humidity, extreme weather conditions and clear-cut on greenhouse gas emissions in fast growing deciduous forests. Tartu, 2016, 128 p.
62. **Mari Nuga.** Soviet-era summerhouses On homes and planning in post-socialist suburbia. Tartu, 2016, 179 p.

63. **Age Poom.** Spatial aspects of the environmental load of consumption and mobility. Tartu, 2017, 141 p.
64. **Merle Muru.** GIS-based palaeogeographical reconstructions of the Baltic Sea shores in Estonia and adjoining areas during the Stone Age. Tartu, 2017, 132 p.
65. **Ülle Napa.** Heavy metals in Estonian coniferous forests. Tartu, 2017, 129 p.
66. **Liisi Jakobson.** Mutual effects of wind speed, air temperature and sea ice concentration in the Arctic and their teleconnections with climate variability in the eastern Baltic Sea region. Tartu, 2018, 118 p.
67. **Tanel Tamm.** Use of local statistics in remote sensing of grasslands and forests. Tartu, 2018, 106 p.
68. **Enel Pungas.** Differences in Migration Intentions by Ethnicity and Education: The Case of Estonia. Tartu, 2018, 142 p.
69. **Kadi Mägi.** Ethnic residential segregation and integration of the Russian-speaking population in Estonia. Tartu, 2018, 173 p.
70. **Kiira Mõisja.** Thematic accuracy and completeness of topographic maps. Tartu, 2018, 112 p.
71. **Kristiina Kukk.** Understanding the vicious circle of segregation: The role of leisure time activities. Tartu, 2019, 143 p.
72. **Kaie Kriiska.** Variation in annual carbon fluxes affecting the soil organic carbon pool and the dynamics of decomposition in hemiboreal coniferous forests. Tartu, 2019, 146 p.
73. **Pille Metspalu.** The changing role of the planner. Implications of creative pragmatism in Estonian spatial planning. Tartu, 2019, 128 p.
74. **Janika Raun.** Mobile positioning data for tourism destination studies and statistics. Tartu, 2020, 153 p.
75. **Birgit Viru.** Snow cover dynamics and its impact on greenhouse gas fluxes in drained peatlands in Estonia. Tartu, 2020, 123 p.
76. **Iuliia Burdun.** Improving groundwater table monitoring for Northern Hemisphere peatlands using optical and thermal satellite data. Tartu, 2020, 162 p.
77. **Ingmar Pastak.** Gentrification and displacement of long-term residents in post-industrial neighbourhoods of Tallinn. Tartu, 2021, 141 p.
78. **Veronika Mooses.** Towards a more comprehensive understanding of ethnic segregation: activity space and the vicious circle of segregation. Tartu, 2021, 161 p.
79. **Johanna Pirrus.** Contemporary Urban Policies and Planning Measures in Socialist-Era Large Housing Estates. Tartu, 2021, 142 p.
80. **Gert Veber.** Greenhouse gas fluxes in natural and drained peatlands: spatial and temporal dynamics. Tartu, 2021, 210 p.
81. **Anniki Puura.** Relationships between personal social networks and spatial mobility with mobile phone data. Tartu, 2021, 144 p.
82. **Alisa Krasnova.** Greenhouse gas fluxes in hemiboreal forest ecosystems. Tartu, 2022, 185 p.

83. **Tauri Tampuu.** Synthetic Aperture Radar Interferometry as a tool for monitoring the dynamics of peatland surface. Tartu, 2022, 166 p.
84. **Najmeh Mozaffaree Pour.** Urban Expansion in Estonia: Monitoring, Analysis, and Modeling. Tartu, 2022, 169 p.
85. **Bruno Montibeller**. Evaluating human-induced forest degradation in different biomes using spatial analysis of satellite-derived data. Tartu, 2022, 112 p.
86. **Holger Virro**. Geospatial data harmonization and machine learning for large-scale water quality modelling. Tartu, 2022, 138 p.
87. **Azadeh Rezapour**. The impact of climate change on fine root trait responses of deciduous and coniferous trees. Tartu, 2023, 108 p.
88. **Isaac Newton Kwasi Buo**. Multi-scale thermal Remote Sensing, Machine Learning, and Radiative Flux Modeling to Assess Urban Overheating. Tartu, 2023, 116 p.
89. **David Knapp**. The relationship between residential segregation, school segregation and family context. Tartu, 2024, 122 p.
90. **Reti Ranniku**. Impact of environmental conditions and soil microbiome on greenhouse gas fluxes from soil and tree stems in hemiboreal drained peatland forest. Tartu, 2024, 142 pp.
91. **Kalev Koppel**. Advancing urban and agricultural monitoring using Sentinel-1 synthetic aperture radar data. Tartu, 2025, 119 pp.